E-ISSN 2586-9027
Homepage : https://tci-thaijo.org/index.php/SciTechAsia Science & Technology Asia
Vol.31 No.3 July - September 2026 Page: [14-41]
Original research article

Parameter Estimation for Brownian Motion with Trend Mixed with Two Fractional Brownian Motions

Phisitphong Ketrat, Raywat Tanadkithirun*

Department of Mathematics and Computer Science, Faculty of Science, Chulalongkorn University, Bangkok 10330, Thailand

Received 24 January 2026; Received in revised form 10 July 2026
Accepted 17 July 2026; Available online 30 September 2026

ABSTRACT

This work studies parameter estimation for a stochastic process that combines a Brownian motion with trend and two fractional Brownian motions with distinct Hurst indices. The process is given by $X_t = \mu t + \sigma W_t + \alpha B_t^{H_1} + \beta B_t^{H_2}$, where W is a standard Brownian motion, while B^{H_1} and B^{H_2} are fractional Brownian motions with Hurst indices $0 < H_1 < H_2 < 1$ such that $H_1, H_2 \neq \frac{1}{2}$, with W, B^{H_1}, and B^{H_2} being mutually independent. An ergodic theorem is applied to derive estimators for all unknown parameters and examine the effect of different Borel function selections on the estimator formulations. Numerical simulations are performed to confirm the asymptotic properties of the estimators and to assess their accuracy under various configurations. The estimators are then applied to cryptocurrency data to demonstrate their practical use.

Keywords: Brownian motion; Ergodic theorem; Fractional Brownian motion

1. Introduction

One of the most widely used stochastic processes is standard Brownian motion (Bm), which serves as the foundation for many models in probability theory and mathematical finance. Due to its independent and stationary increments, Bm has been extensively applied in areas such as option pricing and asset return modeling. However, Bm does not capture long-range dependence which is a feature observed in many real-world time series. Fractional Brownian motion (fBm), first introduced by Kolmogorov [1] in 1940, is a natural extension of Bm that allows for correlated increments. When the Hurst parameter $H > \frac{1}{2}$, the increments exhibit positive correlation, reflecting long-range

***Corresponding author:** raywat.t@chula.ac.th doi.org/10.70730/sta.v31i3.263386

dependence and aggregation behavior. Conversely, for $H < \frac{1}{2}$, the increments are negatively correlated, which reflects their anti-persistent behavior; see, for example, [2–4]. Various studies have examined fBm and its applications, including [5–7]. Despite its wide applicability, fBm is neither a semimartingale nor a Markov process, except in the Bm case $\left(H = \frac{1}{2}\right)$, which limits the applicability of classical stochastic calculus techniques.

To address the non-semimartingale nature of fBm while retaining its ability to capture long-range dependence, Cheridito [8] introduced the mixed fractional Brownian motion (mfBm) in 2001, defined as a linear combination of a Bm with an fBm component. This model has been widely studied and applied in finance, computer network modeling, and physics [9–11]. The problem of estimating parameters for mfBm has received significant attention, with various methods being proposed, including the maximum likelihood estimation [12], Powell's optimization algorithm [13], and the approach based on power variations [14]. In the case of mfBm with trend (mfBmT), Dufitinema et al. [15] proposed a parameter estimation method for the process of the form $Y_t = mt + \sigma(B_t + \lambda B_t^H)$, where B is a Bm and B^H is an fBm independent of B. Their method yields explicit maximum likelihood estimators for m and σ, which depend on H and λ, where the latter are first estimated via minimization of the negative log-likelihood. Taking a different approach, in 2021, Kukush et al. [16] applied an ergodic theorem to estimate all parameters simultaneously.

Inspired by the mfBm, Miao et al. [17] introduced the fractional mixed fractional Brownian motion (fmfBm) in 2008 as a linear combination of two independent fBms with distinct Hurst indices H_1 and H_2. The framework was extended to the fmfBm with trend (fmfBmT) by Mishura [18], who applied the maximum likelihood method to estimate only the drift parameter assuming $\frac{1}{2} \leq H_1 < H_2 < 1$ with the additional restriction $H_2 - H_1 > \frac{1}{4}$. Subsequently, Mishura and Voronov [19] generalized this approach to estimate the drift parameter for any $\frac{1}{2} \leq H_1 < H_2 < 1$, removing the above restriction. As the number of stochastic components increases, however, maximum likelihood estimation becomes considerably more difficult to implement. In particular, evaluating the likelihood function generally requires the inversion of a covariance matrix whose entries depend on all unknown model parameters. For models involving multiple fractional Brownian motion components, the covariance structure becomes substantially more complicated, making likelihood-based estimation analytically challenging and computationally demanding. These challenges motivate the use of alternative estimation methods based on ergodic properties. In 2023, Ralchenko and Yakovliev [20] applied the ergodic theorem to estimate all unknown parameters under the assumption $0 < H_1 < H_2 < 1$.

The increasing application of the ergodic theorem in recent years is driven by two main advantages. First, it directly guarantees almost sure convergence, eliminating the need for separate asymptotic verifications. Second, it allows for the simultaneous estimation of all parameters, avoiding the need to estimate them separately, which may potentially result in larger estimation errors. To construct estimators using the ergodic theorem, it is essential to select appropriate Borel functions. While Kukush et al. [16] propose specific choices for the mfBmT, and Ralchenko and Yakovliev [20] do so for the fmfBmT, it is

evident that the explicit form of the estimators is determined by this selection. Indeed, varying these functions leads to different estimator structures, which may potentially affect the efficiency of the estimators.

This work unifies the frameworks of the mfBmT and the fmfBmT by introducing the *Brownian motion with trend mixed with two fractional Brownian motions (BmT2fBm)*, given by

$$X_t = \mu t + \sigma W_t + \alpha B_t^{H_1} + \beta B_t^{H_2}, \quad (1.1)$$

where W is a Bm and B^{H_1} and B^{H_2} are fBms with Hurst indices $0 < H_1 < H_2 < 1$ such that $H_1, H_2 \neq \frac{1}{2}$. To eliminate the cross-moment terms arising from products of the driving processes, W, B^{H_1}, and B^{H_2} are assumed to be mutually independent. This assumption substantially simplifies the theoretical derivations and enables the construction of explicit estimators. Throughout this paper, we assume that $\sigma, \alpha, \beta > 0$ and $\mu \in \mathbb{R}$. The primary objective of this work is to investigate parameter estimation for the BmT2fBm model using the ergodic theorem. Additionally, we examine the influence of the Borel function selection used in the estimation process on the numerical accuracy of the resulting estimators.

The article is organized as follows. Section 2 introduces the construction of estimators and their mathematical formulation. Section 3 presents alternative estimator formulations based on Borel function selections distinct from those in Section 2. Section 4 reports numerical experiments comparing the performance of these formulations. Section 5 illustrates the practical applicability of the proposed estimators using real-world cryptocurrency data. Section 6 concludes with a discussion of the numerical results.

2. Construction of Estimators

In this section, we apply the ergodic theorem to construct estimators for the parameter vector $\theta = (\mu, \sigma^2, \alpha^2, H_1, \beta^2, H_2)$. Let $h > 0$ be fixed, and assume that the process X_t defined in Eq. (1.1) is observed at discrete time points $t_k = kh$, where $k = 0, 1, 2, \ldots$. Unfortunately, the original process X_t is not ergodic, so direct application of the ergodic theorem is not feasible. To overcome this, we need to construct an appropriate ergodic discrete-time process. This process is defined in the following lemma.

Lemma 2.1. *The process*

$$Y_k = X_{(k+1)h} - X_{kh} - \mu h, \quad k = 0, 1, 2, \ldots$$

is ergodic.

Proof. For $i \in \mathbb{N}$ and $H \in (0, 1)$, let $\widetilde{\rho}(i) = \mathrm{Cov}(Y_0, Y_i)$ and

$$\rho(i, H) = \frac{1}{2}\left(|i+1|^{2H} - 2i^{2H} + |i-1|^{2H}\right).$$

We have

$$\begin{aligned}
&\mathbb{E}\left[B_h^H\left(B_{(i+1)h}^H - B_{ih}^H\right)\right] \\
&= \mathbb{E}\left[B_h^H B_{(i+1)h}^H - B_h^H B_{ih}^H\right] \\
&= \frac{1}{2}\left(|h|^{2H} + |(i+1)h|^{2H} - |ih|^{2H}\right) \\
&\quad - \frac{1}{2}\left(|h|^{2H} + |ih|^{2H} - |(i-1)h|^{2H}\right) \\
&= \frac{h^{2H}}{2}\left(|i+1|^{2H} - 2i^{2H} + |i-1|^{2H}\right) \\
&= h^{2H}\rho(i, H).
\end{aligned}$$

Thus,

$$\begin{aligned}
\widetilde{\rho}(i) &= \mathrm{Cov}(Y_0, Y_i) = \mathbb{E}[Y_0 Y_i] \\
&= \mathbb{E}\Big[\left(\sigma W_h + \alpha B_h^{H_1} + \beta B_h^{H_2}\right) \\
&\qquad \times \left(\sigma\left(W_{(i+1)h} - W_{ih}\right)\right.
\end{aligned}$$

$$
\begin{aligned}
&+ \alpha \left(B^{H_1}_{(i+1)h} - B^{H_1}_{ih} \right) \\
&+ \beta \left(B^{H_2}_{(i+1)h} - B^{H_2}_{ih} \right) \Big) \Big] \\
&= \alpha^2 \mathbb{E}\left[B^{H_1}_h \left(B^{H_1}_{(i+1)h} - B^{H_1}_{ih} \right) \right] \\
&\quad + \beta^2 \mathbb{E}\left[B^{H_2}_h \left(B^{H_2}_{(i+1)h} - B^{H_2}_{ih} \right) \right] \\
&= \alpha^2 h^{2H_1} \rho(i, H_1) + \beta^2 h^{2H_2} \rho(i, H_2).
\end{aligned}
$$

Since W, B^{H_1}, and B^{H_2} are centered Gaussian processes with stationary increments, the sequence $\{Y_k,\ k = 0, 1, \dots\}$ is a stationary Gaussian sequence with $\mathbb{E}(Y_k) = 0$. By a classical result of Maruyama [24] (see also Bennedsen et al. [25]), a stationary Gaussian sequence is ergodic if and only if its autocovariance function converges to zero. Therefore, it suffices to show that $\widetilde{\rho}(i) \to 0$ as $i \to \infty$. Using the fact that for any $H \in (0,1)$, $\rho(i, H) \sim H(2H-1)\, i^{2H-2}$ as $i \to \infty$, we obtain

$$
\begin{aligned}
\widetilde{\rho}(i) &\sim \alpha^2 h^{2H_1} H_1 (2H_1 - 1) i^{2H_1 - 2} \\
&\quad + \beta^2 h^{2H_2} H_2 (2H_2 - 1) i^{2H_2 - 2} \\
&\to 0 \quad \text{as} \quad i \to \infty.
\end{aligned}
$$

Hence, the process $\{Y_k\}_{k \geq 0}$ is ergodic. □

Lemma 2.1 enables us to apply the ergodic theorem to construct estimators following the approach of [16, 20]. Specifically, for a Borel function $g : \mathbb{R}^{l+1} \to \mathbb{R}$ satisfying $\mathbb{E}\,|g(Y_0, Y_1, \dots, Y_l)| < \infty$,we obtain the convergence

$$
\frac{1}{N} \sum_{k=0}^{N-1} g\left(Y_k, Y_{k+1}, \dots, Y_{k+l}\right) \to \mathbb{E}\left(g\left(Y_0, Y_1, \dots, Y_l\right)\right) \text{ a.s. as } N \to \infty. \tag{2.1}
$$

The key idea in constructing estimators is to select appropriate Borel functions g and solve the resulting system of equations. To formalize this approach, we introduce the following notations, adapted from Kukush et al. [16] and Ralchenko and Yakovliev [20]. For all $N \in \mathbb{N}$, define

$$
\nu_N = \frac{1}{N} \sum_{k=0}^{N-1} \left(X_{(k+1)h} - X_{kh} \right)^2, \tag{2.2}
$$

$$
\eta_N = \frac{1}{N} \sum_{k=0}^{N-1} \left(X_{(k+1)h} - X_{kh} \right) \left(X_{(k+2)h} - X_{(k+1)h} \right), \tag{2.3}
$$

$$
\lambda_N = \frac{1}{N} \sum_{k=0}^{N-1} \left(X_{(k+2)h} - X_{kh} \right) \left(X_{(k+4)h} - X_{(k+2)h} \right), \tag{2.4}
$$

$$
\gamma_N = \frac{1}{N} \sum_{k=0}^{N-1} \left(X_{(k+4)h} - X_{kh} \right) \left(X_{(k+8)h} - X_{(k+4)h} \right), \tag{2.5}
$$

$$
\kappa_N = \frac{1}{N} \sum_{k=0}^{N-1} \left(X_{(k+8)h} - X_{kh} \right) \left(X_{(k+16)h} - X_{(k+8)h} \right), \tag{2.6}
$$

and define

$$
\begin{aligned}
\nu_0 &= X_h^2, \\
\eta_0 &= X_h (X_{2h} - X_h), \\
\lambda_0 &= X_{2h} (X_{4h} - X_{2h}), \\
\gamma_0 &= X_{4h} (X_{8h} - X_{4h}), \\
\kappa_0 &= X_{8h} (X_{16h} - X_{8h}).
\end{aligned}
$$

Lemma 2.2. *The following a.s. convergences hold as $N \to \infty$:*

(i) $\dfrac{X_{Nh}}{N} \to \mu h =: f_1(\theta)$,

(ii) $\nu_N \to$

$$
\begin{aligned}
\mathbb{E}(\nu_0) &= \mu^2 h^2 + \sigma^2 h + \alpha^2 h^{2H_1} + \beta^2 h^{2H_2} \\
&=: f_2(\theta),
\end{aligned}
$$

(iii) $\eta_N \to$

$$
\begin{aligned}
\mathbb{E}(\eta_0) &= \mu^2 h^2 + \alpha^2 h^{2H_1} \left(2^{2H_1 - 1} - 1 \right) \\
&\quad + \beta^2 h^{2H_2} \left(2^{2H_2 - 1} - 1 \right)
\end{aligned}
$$

$$=: f_3(\theta),$$

(iv) $\lambda_N \to$

$$\begin{aligned}\mathbb{E}(\lambda_0) &= 4\mu^2h^2 \\ &\quad + \alpha^2h^{2H_1}2^{2H_1}\left(2^{2H_1-1}-1\right) \\ &\quad + \beta^2h^{2H_2}2^{2H_2}\left(2^{2H_2-1}-1\right) \\ &=: f_4(\theta),\end{aligned}$$

(v) $\gamma_N \to$

$$\begin{aligned}\mathbb{E}(\gamma_0) &= 16\mu^2h^2 \\ &\quad + \alpha^2h^{2H_1}2^{4H_1}\left(2^{2H_1-1}-1\right) \\ &\quad + \beta^2h^{2H_2}2^{4H_2}\left(2^{2H_2-1}-1\right) \\ &=: f_5(\theta),\end{aligned}$$

(vi) $\kappa_N \to$

$$\begin{aligned}\mathbb{E}(\kappa_0) &= 64\mu^2h^2 \\ &\quad + \alpha^2h^{2H_1}2^{6H_1}\left(2^{2H_1-1}-1\right) \\ &\quad + \beta^2h^{2H_2}2^{6H_2}\left(2^{2H_2-1}-1\right) \\ &=: f_6(\theta).\end{aligned}$$

Proof. (i) Applying Eq. (2.1) with $g(y_0) = y_0 + \mu h$ yields

$$\frac{1}{N}\sum_{k=0}^{N-1}(Y_k + \mu h) \to \mathbb{E}[Y_0 + \mu h]$$

$$\frac{1}{N}\sum_{k=0}^{N-1}\left(X_{(k+1)h} - X_{kh}\right) \to \mathbb{E}[X_h - X_0]$$

$$\frac{1}{N}\left(X_{Nh} - X_0\right) \to \mathbb{E}[X_h] - \mathbb{E}[X_0]$$

$$\frac{X_{Nh}}{N} \to \mu h$$

a.s. as $N \to \infty$.

(ii) Setting $g(y_0) = (y_0+\mu h)^2$ and applying Eq. (2.1), we obtain

$$\begin{aligned}\nu_N &= \frac{1}{N}\sum_{k=0}^{N-1}\left(X_{(k+1)h} - X_{kh}\right)^2 \\ &\to \mathbb{E}\left[X_h^2\right] \\ &= \mathbb{E}\left[\left(\mu h + \sigma W_h + \alpha B_h^{H_1} + \beta B_h^{H_2}\right)^2\right] \\ &= \mu^2h^2 + \sigma^2\mathbb{E}\left[W_h^2\right] + \alpha^2\mathbb{E}\left[\left(B_h^{H_1}\right)^2\right] \\ &\quad + \beta^2\mathbb{E}\left[\left(B_h^{H_2}\right)^2\right] \\ &= \mu^2h^2 + \sigma^2h + \alpha^2h^{2H_1} + \beta^2h^{2H_2}\end{aligned}$$

a.s. as $N \to \infty$.

(iii) Using $g(y_0, y_1) = (y_0 + \mu h)(y_1 + \mu h)$, we get

$$\begin{aligned}\eta_N &\to \mathbb{E}\left[X_h(X_{2h} - X_h)\right] \\ &= \mathbb{E}\Big[\left(\mu h + \sigma W_h + \alpha B_h^{H_1} + \beta B_h^{H_2}\right) \\ &\quad \times \Big(\mu h + \sigma\left(W_{2h} - W_h\right) \\ &\quad + \alpha\left(B_{2h}^{H_1} - B_h^{H_1}\right) \\ &\quad + \beta\left(B_{2h}^{H_2} - B_h^{H_2}\right)\Big)\Big] \\ &= \mu^2h^2 + \alpha^2\mathbb{E}\left[B_h^{H_1}\left(B_{2h}^{H_1} - B_h^{H_1}\right)\right] \\ &\quad + \beta^2\mathbb{E}\left[B_h^{H_2}\left(B_{2h}^{H_2} - B_h^{H_2}\right)\right]\end{aligned}$$

a.s. as $N \to \infty$. Since $\mathbb{E}\left(B_h^H\left(B_{2h}^H - B_h^H\right)\right)$ $= \mathbb{E}\left(B_h^HB_{2h}^H - \left(B_h^H\right)^2\right) = h^{2H}\left(2^{2H-1}-1\right)$ for all $H \in (0,1)$,

$$\begin{aligned}\eta_N &\to \mu^2h^2 + \alpha^2h^{2H_1}\left(2^{2H_1-1}-1\right) \\ &\quad + \beta^2h^{2H_2}\left(2^{2H_2-1}-1\right)\end{aligned}$$

a.s. as $N \to \infty$.

Following the same approach as in (iii), setting g as

$$\begin{aligned}g(y_0,\ldots,y_3) &= (y_0 + y_1 + 2\mu h) \\ &\quad \times (y_2 + y_3 + 2\mu h), \\ g(y_0,\ldots,y_7) &= (y_0 + \cdots + y_3 + 4\mu h) \\ &\quad \times (y_4 + \cdots + y_7 + 4\mu h), \\ g(y_0,\ldots,y_{15}) &= (y_0 + \cdots + y_7 + 8\mu h) \\ &\quad \times (y_8 + \cdots + y_{15} + 8\mu h),\end{aligned}$$

for (iv), (v), and (vi), respectively, yields the required convergences. □

Next, we introduce the function $f(\theta) \coloneqq \big(f_1(\theta), f_2(\theta), f_3(\theta), f_4(\theta), f_5(\theta), f_6(\theta)\big)$ and define the sequences, for $N \in \mathbb{N}$,

$$\tau_N \coloneqq \left(\frac{X_{Nh}}{N}, \nu_N, \eta_N, \lambda_N, \gamma_N, \kappa_N\right),$$
$$\tau_0 \coloneqq \big(\mu h, \mathbb{E}(\nu_0), \mathbb{E}(\eta_0), \mathbb{E}(\lambda_0), \mathbb{E}(\gamma_0), \mathbb{E}(\kappa_0)\big).$$

Since $f(\theta) = \tau_0$, obtaining estimators for the parameters $(\mu, \sigma^2, \alpha^2, H_1, \beta^2, H_2)$ requires constructing a function q such that

$$q(\tau_0) = \theta. \tag{2.7}$$

The corresponding estimators are then given by $\left(\widehat{\mu}_N, \widehat{\sigma}^2_N, \widehat{\alpha}^2_N, \widehat{H}^{(1)}_N, \widehat{\beta}^2_N, \widehat{H}^{(2)}_N\right) \coloneqq q(\tau_N)$. In other words, to construct strongly consistent estimators, we must solve the estimation equation

$$f(\theta) = \tau_N \tag{2.8}$$

with respect to the unknown parameters. Before presenting the explicit solution, we define the following auxiliary functions:

$$\log_{2+}(x) = \begin{cases} \log_2(x), & \text{if } x > 0, \\ 0, & \text{if } x \le 0, \end{cases} \quad \text{and}$$
$$(x)^{1/2}_+ = \begin{cases} \sqrt{x}, & \text{if } x > 0, \\ 0, & \text{if } x \le 0. \end{cases}$$

Note that for $x > 0$, these functions coincide with the standard $\log_2(x)$ and $\sqrt{x}$, respectively. With these definitions, the explicit solution leads to the following result.

Theorem 2.3. *The The estimator vector* $\widehat{\theta} = \left(\widehat{\mu}_N, \widehat{\sigma}^2_N, \widehat{\alpha}^2_N, \widehat{H}^{(1)}_N, \widehat{\beta}^2_N, \widehat{H}^{(2)}_N\right)$ *is a strongly consistent estimator of* θ *where*

$$\widehat{\mu}_N = \frac{X_{Nh}}{Nh}, \tag{2.9}$$
$$\widehat{H}^{(1)}_N = \frac{1}{2}\log_{2+}(\widehat{x}_N), \tag{2.10}$$
$$\widehat{H}^{(2)}_N = \frac{1}{2}\log_{2+}(\widehat{y}_N), \tag{2.11}$$
$$\widehat{\alpha}^2_N = \frac{\widehat{u}_N}{\widehat{x}_N^{\log_2(h)}}, \tag{2.12}$$
$$\widehat{\beta}^2_N = \frac{\widehat{v}_N}{\widehat{y}_N^{\log_2(h)}}, \tag{2.13}$$
$$\widehat{\sigma}^2_N = \frac{\nu_N - \widehat{\mu}^2_N h^2 - \widehat{u}_N - \widehat{v}_N}{h}, \tag{2.14}$$

with

$$\widehat{a}_N = \eta_N - \widehat{\mu}^2_N h^2, \quad \widehat{b}_N = \lambda_N - 4\widehat{\mu}^2_N h^2,$$
$$\widehat{c}_N = \gamma_N - 16\widehat{\mu}^2_N h^2,$$
$$\widehat{d}_N = \kappa_N - 64\widehat{\mu}^2_N h^2,$$
$$\widehat{D}_N = (\widehat{a}_N\widehat{d}_N - \widehat{b}_N\widehat{c}_N)^2 - 4(\widehat{b}^2_N - \widehat{a}_N\widehat{c}_N)(\widehat{c}^2_N - \widehat{b}_N\widehat{d}_N),$$

$$\widehat{x}_N = \begin{cases} \dfrac{\widehat{b}_N\widehat{c}_N - \widehat{a}_N\widehat{d}_N - (\widehat{D}_N)^{1/2}_+}{2(\widehat{b}^2_N - \widehat{a}_N\widehat{c}_N)}, \\ \qquad \textit{if } H_1 < \dfrac{1}{2} \textit{ and } H_2 > \dfrac{1}{2} \\ \dfrac{\widehat{b}_N\widehat{c}_N - \widehat{a}_N\widehat{d}_N + (\widehat{D}_N)^{1/2}_+}{2(\widehat{b}^2_N - \widehat{a}_N\widehat{c}_N)}, \\ \qquad \textit{otherwise} \end{cases},$$

$$\widehat{y}_N = \begin{cases} \dfrac{\widehat{b}_N\widehat{c}_N - \widehat{a}_N\widehat{d}_N + (\widehat{D}_N)^{1/2}_+}{2(\widehat{b}^2_N - \widehat{a}_N\widehat{c}_N)}, \\ \qquad \textit{if } H_1 < \dfrac{1}{2} \textit{ and } H_2 > \dfrac{1}{2} \\ \dfrac{\widehat{b}_N\widehat{c}_N - \widehat{a}_N\widehat{d}_N - (\widehat{D}_N)^{1/2}_+}{2(\widehat{b}^2_N - \widehat{a}_N\widehat{c}_N)}, \\ \qquad \textit{otherwise} \end{cases},$$

$$\widehat{r}_N = \frac{\widehat{x}_N}{2} - 1, \quad \widehat{s}_N = \frac{\widehat{y}_N}{2} - 1,$$
$$\widehat{u}_N = -\frac{\widehat{b}_N - \widehat{a}_N\widehat{y}_N}{(\widehat{y}_N - \widehat{x}_N)\widehat{r}_N}, \quad \textit{and}$$
$$\widehat{v}_N = \frac{\widehat{b}_N - \widehat{a}_N\widehat{x}_N}{(\widehat{y}_N - \widehat{x}_N)\widehat{s}_N}.$$

Proof. To solve Eq. (2.8), we denote $\nu = \nu_N$, $\eta = \eta_N$, $\lambda = \lambda_N$, $\gamma = \gamma_N$, and $\kappa = \kappa_N$, and define the auxiliary variables as follows: $a = \eta - \mu^2 h^2$, $b = \lambda - 4\mu^2 h^2$, $c = \gamma - 16\mu^2 h^2$, $d = \kappa - 64\mu^2 h^2$, $u = \alpha^2 h^{2H_1}$, $v = \beta^2 h^{2H_2}$, $x = 2^{2H_1}$, $y = 2^{2H_2}$, $r = x/2 - 1$, and $s = y/2 - 1$. With these notations, Eq. (2.8) takes the form

$$\frac{X_{Nh}}{N} = \mu h, \tag{2.15}$$

$$\nu - \mu^2 h^2 = \sigma^2 h + u + v, \tag{2.16}$$

$$a = ur + vs, \tag{2.17}$$

$$b = uxr + vys, \tag{2.18}$$

$$c = ux^2 r + vy^2 s, \tag{2.19}$$

$$d = ux^3 r + vy^3 s. \tag{2.20}$$

It is clear from Eq. (2.15) that

$$\mu = \frac{X_{Nh}}{Nh}. \tag{2.21}$$

Next, we solve for x and y. From Eq. (2.17), we have

$$ax = uxr + vxs \quad \text{and} \quad ay = uyr + vys. \tag{2.22}$$

Using Eq. (2.18) together with Eq. (2.22), we obtain

$$v = \frac{b - ax}{(y - x)s} \quad \text{and} \quad u = -\frac{b - ay}{(y - x)r}. \tag{2.23}$$

Substituting Eq. (2.23) into Eq. (2.19) and Eq. (2.20), we get

$$\begin{aligned} c &= \frac{1}{y - x}\left(b(y^2 - x^2) - axy(y - x)\right) \\ &= b(y + x) - axy, \end{aligned} \tag{2.24}$$

$$\begin{aligned} d &= \frac{1}{y - x}\left(b(y^3 - x^3) - axy(y^2 - x^2)\right) \\ &= b(y^2 + xy + x^2) - axy(y + x), \end{aligned} \tag{2.25}$$

respectively. Multiplying Eq. (2.24) by $y+x$ gives

$$c(x + y) = b(y + x)^2 - axy(y + x). \tag{2.26}$$

Subtracting Eq. (2.25) from Eq. (2.26), we find

$$x = \frac{d - cy}{c - by}, \tag{2.27}$$

$$y = \frac{d - cx}{c - bx}. \tag{2.28}$$

Similarly, from Eq. (2.24),

$$x = \frac{c - by}{b - ay}, \tag{2.29}$$

$$y = \frac{c - bx}{b - ax}. \tag{2.30}$$

Thus, from Eq. (2.27) and Eq. (2.29), we obtain

$$0 = y^2(b^2 - ac) + y(ad - bc) + c^2 - bd.$$

Likewise, from Eq. (2.28) and Eq. (2.30), we get

$$0 = x^2(b^2 - ac) + x(ad - bc) + c^2 - bd.$$

We see that x and y satisfy the same quadratic equation, whose solutions take the form

$$\frac{bc - ad \pm \sqrt{D}}{2(b^2 - ac)}, \tag{2.31}$$

where $D = (ad-bc)^2-4(b^2-ac)(c^2-bd)$. Since

$$\begin{aligned} ad - bc &= uvrs(y - x)^2(y + x), \\ b^2 - ac &= -uvrs(y - x)^2, \\ c^2 - bd &= -uvxyrs(y - x)^2, \end{aligned}$$

we obtain $D = u^2v^2r^2s^2(y - x)^6$. Noting that $u, v, x, y > 0$, $y - x > 0$, and $r, s \neq 0$, it follows that $D > 0$. The case $r > 0$ and $s < 0$ is impossible. For the case $r < 0$ and $s > 0$ (i.e., $H_1 < \frac{1}{2}$ and $H_2 > \frac{1}{2}$), Eq. (2.31) gives

$$\frac{bc - ad \pm \sqrt{D}}{2(b^2 - ac)} = -\frac{1}{2}\left(-y - x \mp (y - x)\right)$$

which leads to

$$x = \frac{bc - ad - \sqrt{D}}{2(b^2 - ac)}, \quad y = \frac{bc - ad + \sqrt{D}}{2(b^2 - ac)}.$$

In the remaining cases where $r, s > 0$ or $r, s < 0$,

$$\frac{bc - ad \pm \sqrt{D}}{2(b^2 - ac)} = -\frac{1}{2}\left(-y - x \pm (y - x)\right).$$

Hence,

$$x = \frac{bc - ad + \sqrt{D}}{2(b^2 - ac)}, \quad y = \frac{bc - ad - \sqrt{D}}{2(b^2 - ac)}.$$

Recalling that $x = 2^{2H_1}$ and $y = 2^{2H_2}$, we obtain

$$H_1 = \frac{1}{2}\log_2(x) \quad \text{and} \quad H_2 = \frac{1}{2}\log_2(y). \tag{2.32}$$

Since $u = \alpha^2 h^{2H_1}$ and $v = \beta^2 h^{2H_2}$, it follows that

$$\alpha^2 = \frac{u}{h^{2H_1}} = \frac{u}{h^{\log_2(x)}} = \frac{u}{x^{\log_2(h)}},$$
$$\beta^2 = \frac{v}{h^{2H_2}} = \frac{v}{h^{\log_2(y)}} = \frac{v}{y^{\log_2(h)}}. \tag{2.33}$$

Finally, from Eq. (2.16), we obtain the expression

$$\sigma^2 = \frac{v - \mu^2 h^2 - u - v}{h}. \tag{2.34}$$

Eqs. (2.21), (2.32)-(2.34) provide the explicit form of the function q in Eq. (2.7). To ensure the continuity of the mapping q at τ_0, we note that all denominators appearing in the explicit expressions remain non-zero under the model assumptions. Indeed, $h > 0$ and $\alpha, \beta > 0$ imply $u, v > 0$, while $0 < H_1 < H_2 < 1$ implies $x = 2^{2H_1} > 0$, $y = 2^{2H_2} > 0$, and $x \neq y$. Moreover, the assumption $H_1, H_2 \neq \frac{1}{2}$ ensures that $r = x/2 - 1 \neq 0$ and $s = y/2 - 1 \neq 0$. Consequently, the denominators in Eq. (2.23) and Eq. (2.31) are non-zero. Since the arguments of the logarithms in Eq. (2.32) are also strictly positive, the mapping q is well-defined and continuous in a neighborhood of τ_0. Thus, replacing τ_0 with τ_N in these equations yields a strongly consistent estimator $\widehat{\theta} = \left(\widehat{\mu}_N, \widehat{\sigma}^2_N, \widehat{\alpha}^2_N, \widehat{H}^{(1)}_N, \widehat{\beta}^2_N, \widehat{H}^{(2)}_N\right)$ for $\theta = \left(\mu, \sigma^2, \alpha^2, H_1, \beta^2, H_2\right)$ as given in Eq. (2.9)–Eq. (2.14). □

Remark 2.4. *The proof relies on the fact that $\widehat{D}_N$, $\widehat{x}_N$, and $\widehat{y}_N$ converge (almost surely) to strictly positive limits as $N \to \infty$. However, for insufficiently large sample sizes, these quantities may occasionally take non-positive values. To prevent computational failures caused by invalid inputs, Theorem 2.3 employs the auxiliary functions $\log_{2+}(\cdot)$ and $(\cdot)^{1/2}_+$. This modification ensures numerical robustness without affecting the theoretical convergence properties. Numerical evidence of such cases is illustrated in Section 4.*

Remark 2.5. *Alternatively, the estimators $\widehat{\alpha}^2_N$, $\widehat{\beta}^2_N$, and $\widehat{\sigma}^2_N$ can be written in terms of $\widehat{\mu}_N$, $\widehat{H}^{(1)}_N$, and $\widehat{H}^{(2)}_N$ as*

$$\widehat{\alpha}^2_N = \frac{\widehat{u}_N}{h^{2\widehat{H}^{(1)}_N}},$$
$$\widehat{\beta}^2_N = \frac{\widehat{v}_N}{h^{2\widehat{H}^{(2)}_N}},$$
$$\widehat{\sigma}^2_N = \frac{v_N - \widehat{\mu}^2_N h^2 - \widehat{\alpha}^2_N h^{2\widehat{H}^{(1)}_N} - \widehat{\beta}^2_N h^{2\widehat{H}^{(2)}_N}}{h}.$$

These expressions define an alternative estimator vector. We conducted extensive numerical experiments and found that this vector yields estimates close to the estimator vector in Theorem 2.3. However, it introduces bias in $\widehat{\alpha}^2_N$, $\widehat{\beta}^2_N$, and $\widehat{\sigma}^2_N$ because their calculation relies on $\widehat{H}^{(1)}_N$ and $\widehat{H}^{(2)}_N$, which are derived using the auxiliary $\log_{2+}(\cdot)$ function. For this reason, we adopt the estimator vector stated in the theorem. Nevertheless, both estimator

vectors become theoretically equivalent as $N \to \infty$.

Remark 2.6. *When applying the estimators to empirical data, the assignment of the two computed roots to* x *and* y *is ambiguous, since the actual values of* H_1 *and* H_2 *are unknown. However, because of our assumption that* $x < y$*, we first compute the two solutions of the roots, then assign the smaller value to* x *and the larger value to* y.

The sequential computational steps for computing the proposed estimators, together with the root-selection procedure described in Remark 2.6, are summarized in Algorithm 1.

3. Alternative Estimator Formulations

As established in Section 2, the explicit expressions for the six estimators are directly determined by the selection of the Borel functions g in Eq. (2.1). In this section, we demonstrate that varying the choice of g allows for the construction of alternative estimators. We specifically propose two approaches to this modification: first, by altering the function selection to affect only the estimator for σ^2 while maintaining the others; and second, by generating a new system of equations to derive distinct estimators.

To illustrate the first approach, we consider the estimators derived in Theorem 2.3 as a baseline. We direct our attention to the estimator for σ^2 because, in the proof of Theorem 2.3, Eq. (2.16) is used exclusively to determine $\widehat{\sigma}_N^2$ and is not required to solve for the other estimators. Thus, replacing this equation yields alternative estimators for σ^2 without affecting the others. Applying arguments similar to those used in the proof of Lemma 2.2, we obtain the following convergences:

$$\begin{aligned}\vartheta_N &:= \frac{1}{N}\sum_{k=0}^{N-1}\left(X_{(k+2)h} - X_{kh}\right)^2 \\ &\to \mu^2(2h)^2 + \sigma^2(2h) + \alpha^2(2h)^{2H_1} \\ &\quad + \beta^2(2h)^{2H_2}, \qquad (3.1)\\ \delta_N &:= \frac{1}{N}\sum_{k=0}^{N-1}\left(X_{(k+4)h} - X_{kh}\right)^2 \\ &\to \mu^2(4h)^2 + \sigma^2(4h) + \alpha^2(4h)^{2H_1} \\ &\quad + \beta^2(4h)^{2H_2}, \qquad (3.2)\\ \varsigma_N &:= \frac{1}{N}\sum_{k=0}^{N-1}\left(X_{(k+8)h} - X_{kh}\right)^2 \\ &\to \mu^2(8h)^2 + \sigma^2(8h) + \alpha^2(8h)^{2H_1} \\ &\quad + \beta^2(8h)^{2H_2}, \qquad (3.3)\\ \psi_N &:= \frac{1}{N}\sum_{k=0}^{N-1}\left(X_{(k+16)h} - X_{kh}\right)^2 \\ &\to \mu^2(16h)^2 + \sigma^2(16h) + \alpha^2(16h)^{2H_1} \\ &\quad + \beta^2(16h)^{2H_2}, \qquad (3.4)\\ \zeta_N &:= \frac{1}{N}\sum_{k=0}^{N-1}\left(X_{(k+1)h} - X_{kh}\right)^3 \\ &\to \mu^3h^3 + 3\mu h^2\sigma^2 + 3\mu h\alpha^2h^{2H_1} \\ &\quad + 3\mu h\beta^2h^{2H_2}. \qquad (3.5)\end{aligned}$$

Replacing Eq. (2.2) with any of these alternatives leads to the following estimators for σ^2, denoted as $\widehat{\sigma}_{k,N}^2$ for $k = 2, \ldots, 6$:

$$\begin{aligned}\widehat{\sigma}_{2,N}^2 &:= \frac{\vartheta_N - \widehat{\mu}_N^2(2h)^2 - \widehat{u}_N\widehat{x}_N - \widehat{v}_N\widehat{y}_N}{2h},\\ \widehat{\sigma}_{3,N}^2 &:= \frac{\delta_N - \widehat{\mu}_N^2(4h)^2 - \widehat{u}_N\widehat{x}_N^2 - \widehat{v}_N\widehat{y}_N^2}{4h},\\ \widehat{\sigma}_{4,N}^2 &:= \frac{\varsigma_N - \widehat{\mu}_N^2(8h)^2 - \widehat{u}_N\widehat{x}_N^3 - \widehat{v}_N\widehat{y}_N^3}{8h},\\ \widehat{\sigma}_{5,N}^2 &:= \frac{\psi_N - \widehat{\mu}_N^2(16h)^2 - \widehat{u}_N\widehat{x}_N^4 - \widehat{v}_N\widehat{y}_N^4}{16h},\\ \widehat{\sigma}_{6,N}^2 &:= \frac{\zeta_N - \widehat{\mu}_N^3h^3 - 3\widehat{\mu}_Nh(\widehat{u}_N + \widehat{v}_N)}{3\widehat{\mu}_Nh^2},\end{aligned}$$

respectively. These values differ slightly from $\widehat{\sigma}_{1,N}^2 := \widehat{\sigma}_N^2$ given in Eq. (2.14), while

Algorithm 1 Sequential Computational Steps for Parameter Estimation (Theorem 2.3)

Input: Discrete observations $X = (X_0, X_h, \ldots, X_{Nh}, \ldots, X_{(N+16)h})$, time step $h > 0$
Step 1: Estimate Trend (μ)
$\widehat{\mu}_N \leftarrow \frac{X_{Nh}}{Nh}$
Step 2: Compute Sample Variations
Compute $\nu_N, \eta_N, \lambda_N, \gamma_N, \kappa_N$ using Equations Eq. (2.2)–Eq. (2.6)
Step 3: Centralize Variations
$m_h \leftarrow \widehat{\mu}_N^2 h^2$
$\widehat{a}_N \leftarrow \eta_N - m_h, \quad \widehat{b}_N \leftarrow \lambda_N - 4m_h, \quad \widehat{c}_N \leftarrow \gamma_N - 16m_h, \quad \widehat{d}_N \leftarrow \kappa_N - 64m_h$
Step 4: Solve for Intermediate Parameters
$\widehat{D}_N \leftarrow (\widehat{a}_N\widehat{d}_N - \widehat{b}_N\widehat{c}_N)^2 - 4(\widehat{b}_N^2 - \widehat{a}_N\widehat{c}_N)(\widehat{c}_N^2 - \widehat{b}_N\widehat{d}_N)$
$\text{den} \leftarrow 2(\widehat{b}_N^2 - \widehat{a}_N\widehat{c}_N)$
$\text{root}_1 \leftarrow \frac{\widehat{b}_N\widehat{c}_N - \widehat{a}_N\widehat{d}_N + (\widehat{D}_N)_+^{1/2}}{\text{den}}$
$\text{root}_2 \leftarrow \frac{\widehat{b}_N\widehat{c}_N - \widehat{a}_N\widehat{d}_N - (\widehat{D}_N)_+^{1/2}}{\text{den}}$
$\widehat{x}_N \leftarrow \min(\text{root}_1, \text{root}_2)$
$\widehat{y}_N \leftarrow \max(\text{root}_1, \text{root}_2)$
Step 5: Compute Final Estimators
$\widehat{r}_N \leftarrow \frac{\widehat{x}_N}{2} - 1, \quad \widehat{s}_N \leftarrow \frac{\widehat{y}_N}{2} - 1$
$\widehat{u}_N \leftarrow -\frac{\widehat{b}_N - \widehat{a}_N\widehat{y}_N}{(\widehat{y}_N - \widehat{x}_N)\widehat{r}_N}$
$\widehat{v}_N \leftarrow \frac{\widehat{b}_N - \widehat{a}_N\widehat{x}_N}{(\widehat{y}_N - \widehat{x}_N)\widehat{s}_N}$
$\widehat{H}_N^{(1)} \leftarrow \frac{1}{2}\log_{2+}(\widehat{x}_N)$
$\widehat{H}_N^{(2)} \leftarrow \frac{1}{2}\log_{2+}(\widehat{y}_N)$
$\widehat{\alpha}_N^2 \leftarrow \frac{\widehat{u}_N}{\widehat{x}_N^{\log_2(h)}}$
$\widehat{\beta}_N^2 \leftarrow \frac{\widehat{v}_N}{\widehat{y}_N^{\log_2(h)}}$
$\widehat{\sigma}_N^2 \leftarrow \frac{\nu_N - m_h - \widehat{u}_N - \widehat{v}_N}{h}$
Output: $(\widehat{\mu}_N, \widehat{\sigma}_N^2, \widehat{\alpha}_N^2, \widehat{H}_N^{(1)}, \widehat{\beta}_N^2, \widehat{H}_N^{(2)})$

leaving the estimators for all other parameters invariant. As we will show in Section 4, the estimated values of σ^2 derived from these modifications remain numerically close to $\widehat{\sigma}_{1,N}^2$. Note, however, that the formulation of $\widehat{\sigma}_{6,N}^2$ involves division by the trend estimator $\widehat{\mu}_N$. Accordingly, its use requires the theoretical assumption that $\mu \neq 0$. Furthermore, even under this assumption, the formula cannot be applied if the computed value of $\widehat{\mu}_N$ is exactly zero. Fortunately, in practice, this event is highly unlikely.

Turning to the second approach, we propose two additional equation systems in Theorems 3.1 and 3.2. In both systems, we retain the original estimator for μ, consistent with Theorem 2.3.

Theorem 3.1. *The estimator vector* $\widetilde{\theta} = \left(\widetilde{\mu}_N, \widetilde{\sigma}_N^2, \widetilde{\alpha}_N^2, \widetilde{H}_N^{(1)}, \widetilde{\beta}_N^2, \widetilde{H}_N^{(2)}\right)$ *is a strongly*

consistent estimator of θ where

$$\begin{aligned}
\widetilde{\mu}_N &= \frac{X_{Nh}}{Nh},\\
\widetilde{H}_N^{(1)} &= \frac{1}{2}\log_{2+}(\widetilde{x}_N),\\
\widetilde{H}_N^{(2)} &= \frac{1}{2}\log_{2+}(\widetilde{y}_N),\\
\widetilde{\alpha}_N^2 &= \frac{\widetilde{u}_N}{\widetilde{x}_N^{\log_2(h)}},\\
\widetilde{\beta}_N^2 &= \frac{\widetilde{v}_N}{\widetilde{y}_N^{\log_2(h)}},\\
\widetilde{\sigma}_N^2 &= \frac{\widetilde{m}_N - \widetilde{u}_N\widetilde{x}_N^2 - \widetilde{v}_N\widetilde{y}_N^2}{4h},
\end{aligned}$$

with

$$\begin{aligned}
&\widetilde{a}_N = \eta_N - \widetilde{\mu}_N^2 h^2, \quad \widetilde{b}_N = \lambda_N - 4\widetilde{\mu}_N^2 h^2,\\
&\widetilde{c}_N = \gamma_N - 16\widetilde{\mu}_N^2 h^2, \widetilde{m}_N = \delta_N - 16\widetilde{\mu}_N^2 h^2,\\
&\widetilde{e}_N = \psi_N - 256\widetilde{\mu}_N^2 h^2,\\
&\widetilde{D}_N = \left[\widetilde{a}_N(\widetilde{e}_N - 4\widetilde{m}_N - 4\widetilde{c}_N) - 2\widetilde{b}_N\widetilde{c}_N\right]^2\\
&\qquad - 8(\widetilde{a}_N\widetilde{c}_N - \widetilde{b}_N^2)\\
&\qquad\quad \times\left[\widetilde{b}_N(\widetilde{e}_N - 4\widetilde{m}_N - 4\widetilde{c}_N) - 2\widetilde{c}_N^2\right],
\end{aligned}$$

$$\widetilde{x}_N = \begin{cases}
\dfrac{\widetilde{a}_N\widetilde{e}_N - 2\widetilde{b}_N\widetilde{c}_N - 4\widetilde{a}_N\widetilde{m}_N - 4\widetilde{a}_N\widetilde{c}_N + (\widetilde{D}_N)_+^{1/2}}{4(\widetilde{a}_N\widetilde{c}_N - \widetilde{b}_N^2)}, \\
\qquad \text{if } H_1 < \dfrac{1}{2} \text{ and } H_2 > \dfrac{1}{2} \\
\dfrac{\widetilde{a}_N\widetilde{e}_N - 2\widetilde{b}_N\widetilde{c}_N - 4\widetilde{a}_N\widetilde{m}_N - 4\widetilde{a}_N\widetilde{c}_N - (\widetilde{D}_N)_+^{1/2}}{4(\widetilde{a}_N\widetilde{c}_N - \widetilde{b}_N^2)}, \\
\qquad \text{otherwise}
\end{cases},$$

$$\widetilde{y}_N = \begin{cases}
\dfrac{\widetilde{a}_N\widetilde{e}_N - 2\widetilde{b}_N\widetilde{c}_N - 4\widetilde{a}_N\widetilde{m}_N - 4\widetilde{a}_N\widetilde{c}_N - (\widetilde{D}_N)_+^{1/2}}{4(\widetilde{a}_N\widetilde{c}_N - \widetilde{b}_N^2)}, \\
\qquad \text{if } H_1 < \dfrac{1}{2} \text{ and } H_2 > \dfrac{1}{2} \\
\dfrac{\widetilde{a}_N\widetilde{e}_N - 2\widetilde{b}_N\widetilde{c}_N - 4\widetilde{a}_N\widetilde{m}_N - 4\widetilde{a}_N\widetilde{c}_N + (\widetilde{D}_N)_+^{1/2}}{4(\widetilde{a}_N\widetilde{c}_N - \widetilde{b}_N^2)}, \\
\qquad \text{otherwise}
\end{cases},$$

$$\begin{aligned}
&\widetilde{r}_N = \frac{\widetilde{x}_N}{2} - 1, \quad \widetilde{s}_N = \frac{\widetilde{y}_N}{2} - 1,\\
&\widetilde{u}_N = -\frac{\widetilde{b}_N - \widetilde{a}_N\widetilde{y}_N}{(\widetilde{y}_N - \widetilde{x}_N)\widetilde{r}_N}, \quad \textit{and}\\
&\widetilde{v}_N = \frac{\widetilde{b}_N - \widetilde{a}_N\widetilde{x}_N}{(\widetilde{y}_N - \widetilde{x}_N)\widetilde{s}_N}.
\end{aligned}$$

Proof. Solving the system given by Eqs. (2.3)-(2.5), (3.2), and Eq. (3.4) as in Theorem 2.3 with auxiliary variables $e = \psi - 256\mu^2h^2$, $m = \delta - 16\mu^2h^2$, and $w = \sigma^2 h$, the system becomes:

$$a = ur + vs, \tag{2.17}$$
$$b = uxr + vys, \tag{2.18}$$
$$c = ux^2r + vy^2s, \tag{2.19}$$
$$e = 16w + ux^4 + vy^4, \tag{3.6}$$
$$m = 4w + ux^2 + vy^2. \tag{3.7}$$

We apply the proof technique of Theorem 2.3. First, we obtain:

$$\begin{aligned}
&u = -\frac{b - ay}{(y - x)r}, \quad v = \frac{b - ax}{(y - x)s},\\
&x = \frac{c - by}{b - ay}, \quad \text{and} \quad y = \frac{c - bx}{b - ax}.
\end{aligned} \tag{3.8}$$

From the above setup, we have $e - 4m = 2cx + 2cy + 4c - 2bxy$, and thus,

$$x = \frac{e - 4m - 2cy - 4c}{2c - 2by} \quad \text{and}$$

$$y = \frac{e - 4m - 2cx - 4c}{2c - 2bx}.$$

We find that x and y satisfy the same quadratic equation

$$\begin{aligned} 0 &= z^2(2ac - 2b^2) \\ &\quad + z(2bc - ae + 4am + 4ac) \\ &\quad + be - 4bc - 4bm - 2c^2 \end{aligned}$$

with solutions given by

$$\frac{ae - 2bc - 4am - 4ac \pm \sqrt{D_2}}{4(ac - b^2)}, \quad (3.9)$$

where $D_2 = (ae - 2bc - 4am - 4ac)^2 - 8(ac - b^2)(be - 4bc - 4bm - 2c^2)$. Upon algebraic simplification, we obtain $D_2 = 4u^2v^2r^2s^2(y - x)^6$. Noting that $u, v, x, y > 0$, $y - x > 0$, and $r, s \neq 0$, it follows that $D_2 > 0$. The case $r > 0$ and $s < 0$ is impossible. For the case $r < 0$ and $s > 0$ (i.e., $H_1 < \frac{1}{2}$ and $H_2 > \frac{1}{2}$), Eq. (3.9) gives

$$\begin{aligned} &\frac{ae - 2bc - 4am - 4ac \pm \sqrt{D_2}}{4(ac - b^2)} \\ &= \frac{1}{2}\left(x + y \mp (y - x)\right) \end{aligned}$$

which leads to

$$\begin{aligned} x &= \frac{ae - 2bc - 4am - 4ac + \sqrt{D_2}}{4(ac - b^2)}, \\ y &= \frac{ae - 2bc - 4am - 4ac - \sqrt{D_2}}{4(ac - b^2)}. \end{aligned}$$

In the remaining cases where $r, s > 0$ or $r, s < 0$,

$$\begin{aligned} &\frac{ae - 2bc - 4am - 4ac \pm \sqrt{D_2}}{4(ac - b^2)} \\ &= \frac{1}{2}\left(x + y \pm (y - x)\right). \end{aligned}$$

Hence,

$$x = \frac{ae - 2bc - 4am - 4ac - \sqrt{D_2}}{4(ac - b^2)},$$

$$y = \frac{ae - 2bc - 4am - 4ac + \sqrt{D_2}}{4(ac - b^2)}.$$

Recalling the definitions $x = 2^{2H_1}$ and $y = 2^{2H_2}$, we obtain

$$H_1 = \frac{1}{2}\log_2(x) \quad \text{and} \quad H_2 = \frac{1}{2}\log_2(y).$$

Since $u = \alpha^2 h^{2H_1}$ and $v = \beta^2 h^{2H_2}$, it follows that

$$\alpha^2 = \frac{u}{x^{\log_2(h)}} \quad \text{and} \quad \beta^2 = \frac{v}{y^{\log_2(h)}}.$$

Finally, from Eq. (3.7), we obtain $4w = m - ux^2 - vy^2$, and since $w = \sigma^2 h$, we have

$$\sigma^2 = \frac{m - ux^2 - vy^2}{4h}.$$

Analogous to Theorem 2.3, all relevant denominators remain strictly non-zero under the model assumptions. Therefore, the associated mapping is continuous at the limit point, and the continuous mapping theorem implies that $\widetilde{\theta}$ is a strongly consistent estimator of θ. □

Theorem 3.2. *The estimator vector* $\breve{\theta} = \left(\breve{\mu}_N, \breve{\sigma}^2_N, \breve{\alpha}^2_N, \breve{H}^{(1)}_N, \breve{\beta}^2_N, \breve{H}^{(2)}_N\right)$ *is a strongly consistent estimator of* θ *where*

$$\begin{aligned} \breve{\mu}_N &= \frac{X_{Nh}}{Nh}, \\ \breve{H}^{(1)}_N &= \frac{1}{2}\log_{2+}(\breve{x}_N), \\ \breve{H}^{(2)}_N &= \frac{1}{2}\log_{2+}(\breve{y}_N), \\ \breve{\alpha}^2_N &= \frac{\breve{u}_N}{\breve{x}_N^{\log_2(h)}}, \\ \breve{\beta}^2_N &= \frac{\breve{v}_N}{\breve{y}_N^{\log_2(h)}}, \\ \breve{\sigma}^2_N &= \frac{\breve{n}_N - \breve{u}_N\breve{x}^3_N - \breve{v}_N\breve{y}^3_N}{8h} \end{aligned}$$

with

$$
\begin{aligned}
\breve{a}_N &= \eta_N - \breve{\mu}_N^2 h^2, \quad \breve{b}_N = \lambda_N - 4\breve{\mu}_N^2 h^2,\\
\breve{c}_N &= \gamma_N - 16\breve{\mu}_N^2 h^2,\\
\breve{n}_N &= \varsigma_N - 64\breve{\mu}_N^2 h^2,\\
\breve{e}_N &= \psi_N - 256\breve{\mu}_N^2 h^2,\\
\breve{D}_N &= (\breve{a}_N\breve{e}_N - 2\breve{b}_N\breve{c}_N - 2\breve{a}_N\breve{n}_N)^2\\
&\quad - 8(\breve{a}_N\breve{c}_N - \breve{b}_N^2)\\
&\quad\quad \times (\breve{b}_N\breve{e}_N - 2\breve{b}_N\breve{n}_N - 2\breve{c}_N^2),
\end{aligned}
$$

$$
\breve{x}_N = \begin{cases}
\dfrac{-2\breve{b}_N\breve{c}_N + (\breve{e}_N - 2\breve{n}_N)\breve{a}_N + (\breve{D}_N)_+^{1/2}}{4(\breve{a}_N\breve{c}_N - \breve{b}_N^2)}, \\
\qquad \textit{if } H_1 < \dfrac{1}{2} \textit{ and } H_2 > \dfrac{1}{2} \\
\dfrac{-2\breve{b}_N\breve{c}_N + (\breve{e}_N - 2\breve{n}_N)\breve{a}_N - (\breve{D}_N)_+^{1/2}}{4(\breve{a}_N\breve{c}_N - \breve{b}_N^2)}, \\
\qquad \textit{otherwise}
\end{cases},
$$

$$
\breve{y}_N = \begin{cases}
\dfrac{-2\breve{b}_N\breve{c}_N + (\breve{e}_N - 2\breve{n}_N)\breve{a}_N - (\breve{D}_N)_+^{1/2}}{4(\breve{a}_N\breve{c}_N - \breve{b}_N^2)}, \\
\qquad \textit{if } H_1 < \dfrac{1}{2} \textit{ and } H_2 > \dfrac{1}{2} \\
\dfrac{-2\breve{b}_N\breve{c}_N + (\breve{e}_N - 2\breve{n}_N)\breve{a}_N + (\breve{D}_N)_+^{1/2}}{4(\breve{a}_N\breve{c}_N - \breve{b}_N^2)}, \\
\qquad \textit{otherwise}
\end{cases},
$$

$$
\begin{aligned}
\breve{r}_N &= \frac{\breve{x}_N}{2} - 1, \quad \breve{s}_N = \frac{\breve{y}_N}{2} - 1,\\
\breve{u}_N &= -\frac{\breve{b}_N - \breve{a}_N\breve{y}_N}{(\breve{y}_N - \breve{x}_N)\breve{r}_N}, \quad \textit{and}\\
\breve{v}_N &= \frac{\breve{b}_N - \breve{a}_N\breve{x}_N}{(\breve{y}_N - \breve{x}_N)\breve{s}_N}.
\end{aligned}
$$

Proof. Solving the system given by Eqs. (2.3)-(2.5), and Eqs. (3.3)-(3.4) as in Theorem 2.3 with auxiliary variables $e = \psi - 256\mu^2h^2$, $n = \varsigma - 64\mu^2h^2$, and $w = \sigma^2 h$, the system becomes:

$$a = ur + vs, \tag{2.17}$$
$$b = uxr + vys, \tag{2.18}$$
$$c = ux^2r + vy^2s, \tag{2.19}$$
$$e = 16w + ux^4 + vy^4, \tag{3.6}$$
$$n = 8w + ux^3 + vy^3. \tag{3.10}$$

Again, we obtain the four equations given in Eq. (3.8). Subtracting 2 times Eq. (3.10) from Eq. (3.6), we have $e-2n = 2cx+2cy-2bxy$, and thus,

$$x = \frac{e - 2n - 2cy}{2c - 2by} \quad \text{and} \quad y = \frac{e - 2n - 2cx}{2c - 2bx}.$$

Hence, x and y satisfy the same quadratic equation

$$0 = z^2(2ac - 2b^2) + z(2bc - ae + 2an) + be - 2bn - 2c^2$$

with solutions given by

$$\frac{-2bc + (e - 2n)a \pm \sqrt{D_3}}{4(ac - b^2)}, \tag{3.11}$$

where $D_3 = (2bc - ae + 2an)^2 - 8(ac - b^2)(be-2bn-2c^2)$. Upon algebraic simplification, we obtain $D_3 = 4u^2v^2r^2s^2(y-x)^6$. Noting that $u, v, x, y > 0$, $y - x > 0$, and $r, s \neq 0$, it follows that $D_3 > 0$. Applying the same root selection logic as in Theorem 3.1, Eq. (3.11) yields the expressions for $\breve{x}_N$ and $\breve{y}_N$ given in the theorem. Recalling the definitions $x = 2^{2H_1}$ and $y = 2^{2H_2}$, we obtain

$$H_1 = \frac{1}{2}\log_2(x) \quad \text{and} \quad H_2 = \frac{1}{2}\log_2(y).$$

Since $u = \alpha^2 h^{2H_1}$ and $v = \beta^2 h^{2H_2}$, it follows that

$$\alpha^2 = \frac{u}{x^{\log_2(h)}} \quad \text{and} \quad \beta^2 = \frac{v}{y^{\log_2(h)}}.$$

Finally, from Eq. (3.10), we obtain $8w = n - ux^3 - vy^3$, and since $w = \sigma^2 h$, we acquire

$$\sigma^2 = \frac{n - ux^3 - vy^3}{8h}.$$

Analogous to Theorem 2.3, all relevant denominators remain strictly non-zero under the model assumptions. Therefore, the associated mapping is continuous at the limit point, and the continuous mapping theorem implies that $\breve{\theta}$ is a strongly consistent estimator of θ. □

Remark 3.3. *In solving the system for w in order to derive the estimator for σ^2, Eq.* (3.6) *could alternatively be employed. However, we utilized Eq.* (3.7) *and Eq.* (3.10) *for this purpose in Theorems 3.1 and 3.2, respectively. This specific choice of the equation for σ^2 does not affect the strong consistency of the resulting estimator vectors $\widetilde{\theta}$ and $\breve{\theta}$, as will be discussed in Section 4.3.*

Remark 3.4. *Consider the set of nine equations provided by Eq.* (2.2)*–Eq.* (2.6) *and Eq.* (3.1)*–Eq.* (3.4)*, with Eq.* (3.5) *omitted due to its algebraic complexity. Since μ can be estimated separately, five unknown parameters remain to be identified. Constructing an estimation system therefore requires the selection of exactly five equations, resulting in a total of $\binom{9}{5} = 126$ possible combinations. By examining all 126 possible systems, we found that only seven admit explicit closed-form solutions. Inspection of these seven successful systems indicates that they all possess an algebraic structure that enables the analytical elimination of the linear variables u and v (corresponding to α^2 and β^2), thereby reducing the remaining equations to a quadratic system in $x = 2^{2H_1}$ and $y = 2^{2H_2}$, which can be solved explicitly. For the remaining combinations, obtaining such an analytical reduction is considerably more difficult. Instead, the resulting systems involve more strongly coupled nonlinear equations that do not readily admit explicit closed-form solutions. For these remaining combinations, the resulting nonlinear systems may be solved numerically using root-finding procedures such as Newton-type methods. However, numerical approaches for multidimensional nonlinear systems often depend strongly on the choice of initial values and may suffer from convergence difficulties. Therefore, to ensure computational efficiency, maintain explicit analytical expressions, and preserve theoretical tractability, this paper focuses exclusively on the seven systems that admit explicit solutions. These successful combinations yield the estimator vectors presented in Theorems 3.1 and 3.2, together with five variants based on Theorem 2.3. In these five variants, the estimator for σ^2 is chosen from the set $\{\widehat{\sigma}^2_{k,N}\}_{k=1}^5$, while the other estimators remain invariant.*

4. Numerical Simulations

In this section, we conduct numerical simulations to evaluate the performance of the proposed estimators. To simulate trajectories of the BmT2fBm model, we generate Bm and fBms. The Bm is simulated using standard techniques (see, e.g., Higham [21]). The fractional Gaussian noise is synthesized using the simulation procedure described by Shevchenko [22], which is based on the exact circulant embedding method originally proposed by

Wood and Chan [23]. Subsequently, the paths of the fBms are obtained by computing the cumulative sums of the fractional Gaussian noise. In this simulation framework, the number of generated fBm samples is constrained to powers of two. Because of this condition, setting $N = 2^q$ would necessitate simulating 2^{q+1} points to accommodate estimator lags. To avoid this computational overhead, we fix $T = 2^q$ and set $N = T - 15$. This adjustment is computationally efficient and asymptotically negligible.

4.1 Numerical Verification of Strong Consistency

The strong consistency of the estimators derived in Theorem 2.3 is verified through a Monte Carlo study. Since the Hurst indices significantly influence the sample path behavior of the model, we design the experiment to assess performance across a diverse range of index combinations. In this analysis, sample paths of the BmT2fBm process are simulated using a fixed step size of $h = 1$ and constant model parameters: $\mu = 0.5$, $\sigma = 1.5$, $\alpha = 2.5$, and $\beta = 2.0$. To clearly observe the asymptotic behavior of the estimators, we vary the sample size exponent $q = 14, 16, 18, 20, 22$ (where $T = 2^q$) alongside the following pairs of Hurst parameters (H_1, H_2): $(0.1, 0.3)$, $(0.1, 0.6)$, $(0.1, 0.9)$, $(0.3, 0.6)$, $(0.3, 0.9)$, $(0.4, 0.7)$, $(0.4, 0.9)$, $(0.6, 0.9)$, and $(0.7, 0.9)$. Based on 1000 independent simulations for each parameter combination, we report the averaged values of the six estimators $\widehat{\mu}_N, \widehat{H}_N^{(1)}, \widehat{H}_N^{(2)}, \widehat{\alpha}_N^2, \widehat{\beta}_N^2$, and $\widehat{\sigma}_N^2$ in Table 1 and Table 2. Additionally, to visually illustrate the strong consistency of the proposed estimators, Fig. 1 plots these averaged values as the sample size increases for representative pairs of Hurst parameters.

The convergence of the trend estimator $\widehat{\mu}_N$ is examined in Table 1. The averaged values remain consistently close to the true value $\mu = 0.5$ across all tested (H_1, H_2) pairs and sample size exponents q. These results demonstrate the robust performance of the estimator, which achieves high accuracy even at the lowest sample size considered and exhibits clear asymptotic convergence as N increases.

The strong consistency of $\widehat{H}_N^{(1)}$ and $\widehat{H}_N^{(2)}$ is demonstrated in Table 2. We observe persistently negative averaged values for $\widehat{H}_N^{(1)}$ in the $(0.1, 0.3)$ pair and a negative averaged value in the $(0.3, 0.6)$ pair. Moreover, some averaged values for $\widehat{H}_N^{(2)}$ exceed 1 in the $(0.6, 0.9)$ and $(0.7, 0.9)$ pairs. These out-of-bounds estimates are primarily associated with certain configurations of the Hurst parameters, as will be discussed in Section 4.2. Apart from the fluctuations observed in the averaged estimates, a closer inspection of individual sample paths reveals that in some cases, the value of $\widehat{H}_N^{(1)}$ is exactly equal to $\widehat{H}_N^{(2)}$. This is caused by non-positive values of the discriminant $\widehat{D}_N$, which forces the roots $\widehat{x}_N$ and $\widehat{y}_N$ to be equal. We denote the frequency of these occurrences as $N_{D\leq 0}$. Crucially, a non-zero $N_{D\leq 0}$ does not inherently invalidate the computed values of $\widehat{H}_N^{(1)}$ and $\widehat{H}_N^{(2)}$, as the accuracy of their averaged values remains robust even when the roots coincide. We observe that $N_{D\leq 0}$ decreases significantly as q increases; however, it remains positive for the $(0.3, 0.6)$ and $(0.4, 0.7)$ pairs even at $q = 22$.

We now turn to the verification of strong consistency for the coefficient estimators $\widehat{\alpha}_N^2$, $\widehat{\beta}_N^2$, and $\widehat{\sigma}_N^2$, with results summarized in Table 2. Based on the behavior at $q = 22$, the Hurst pa-

Table 1. Averaged values of $\widehat{\mu}_N$ across 1000 Monte Carlo paths with varying q. The true parameters are $\mu = 0.5, \sigma = 1.5, \alpha = 2.5$, and $\beta = 2$, with $h = 1$.

		q				
H_1	H_2	14	16	18	20	22
0.1	0.3	0.50052	0.50009	0.50001	0.49999	0.50001
0.1	0.6	0.50170	0.50132	0.50079	0.50004	0.50001
0.1	0.9	0.52853	0.52679	0.52885	0.50200	0.50250
0.3	0.6	0.50164	0.50128	0.50077	0.50004	0.50001
0.3	0.9	0.52847	0.52675	0.52884	0.50200	0.50250
0.4	0.7	0.50377	0.50358	0.50262	0.50019	0.50004
0.4	0.9	0.52832	0.52667	0.52878	0.50202	0.50249
0.6	0.9	0.52671	0.52593	0.52778	0.50224	0.50226
0.7	0.9	0.52348	0.52451	0.52496	0.50299	0.50149

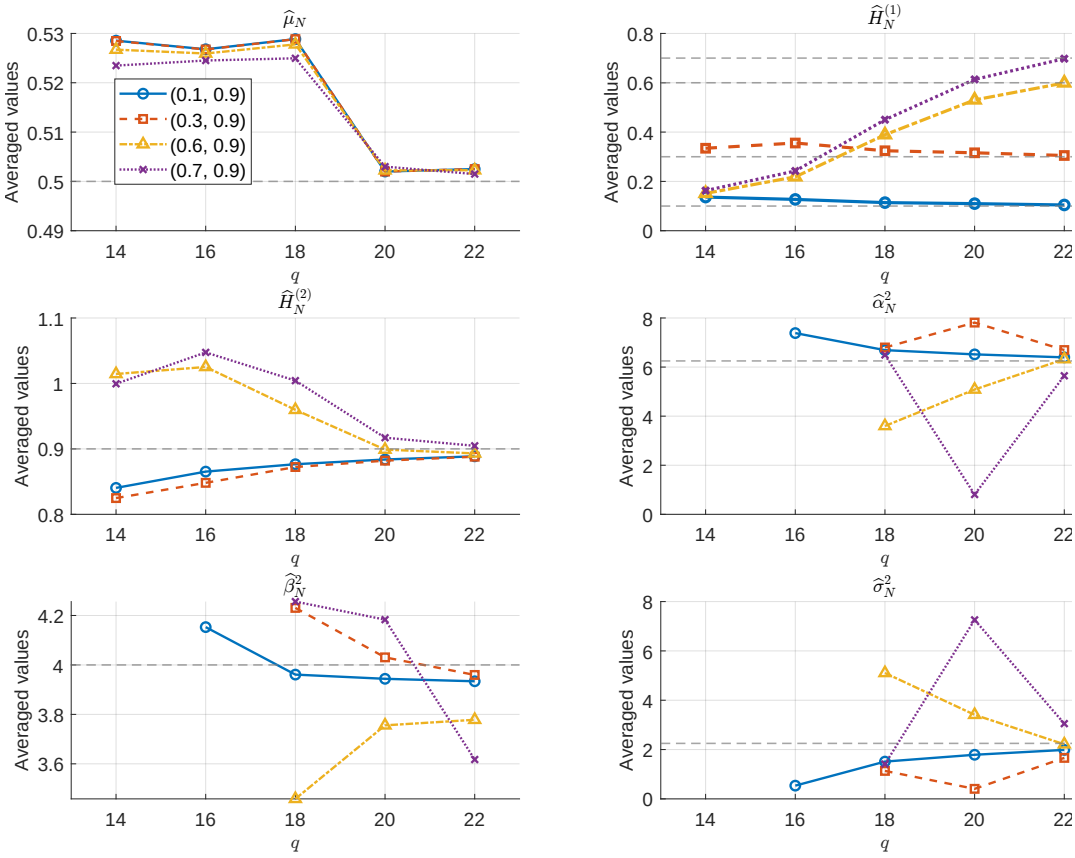


Fig. 1. Averaged values of the proposed estimators for representative Hurst parameter pairs: $(0.1, 0.9)$, $(0.3, 0.9)$, $(0.6, 0.9)$, and $(0.7, 0.9)$ as the sample size exponent q increases. The dashed horizontal lines indicate the corresponding true parameter values. The true model parameters are $\mu = 0.5$, $\sigma = 1.5$, $\alpha = 2.5$, and $\beta = 2$, with $h = 1$.

rameter pairs can be classified into three categories: (1) those exhibiting valid numerical convergence toward the true parameters; (2) those yielding *special-*

Table 2. Consolidated averaged values of $\widehat{H}_N^{(1)}$, $\widehat{H}_N^{(2)}$, $\widehat{\alpha}_N^2$, $\widehat{\beta}_N^2$, and $\widehat{\sigma}_N^2$, along with the count $N_{D\leq 0}$, across 1000 Monte Carlo paths with varying q. The true parameters are $\mu = 0.5, \sigma = 1.5, \alpha = 2.5$, and $\beta = 2$, with $h = 1$.

H_1	H_2		q					True Value
			14	16	18	20	22	
0.1	0.3	$\widehat{H}_N^{(1)}$	-0.06301	-0.10365	-0.13134	-0.15869	-0.03021	0.1
		$\widehat{H}_N^{(2)}$	0.37869	0.41678	0.46422	0.49483	0.41950	0.3
		$\widehat{\alpha}_N^2$	NaN	NaN	-Inf	4.46321	5.26272	6.25
		$\widehat{\beta}_N^2$	NaN	NaN	Inf	5.37423	5.10819	4
		$\widehat{\sigma}_N^2$	NaN	NaN	NaN	2.66234	2.12887	2.25
		$N_{D\leq 0}$	28	9	1	0	0	-
0.1	0.6	$\widehat{H}_N^{(1)}$	0.00142	0.10450	0.11960	0.11217	0.10310	0.1
		$\widehat{H}_N^{(2)}$	0.58882	0.55093	0.57372	0.58586	0.59656	0.6
		$\widehat{\alpha}_N^2$	NaN	NaN	Inf	Inf	6.48045	6.25
		$\widehat{\beta}_N^2$	NaN	NaN	-Inf	-Inf	24.41964	4
		$\widehat{\sigma}_N^2$	NaN	NaN	NaN	NaN	-18.40021	2.25
		$N_{D\leq 0}$	417	343	179	42	0	-
0.1	0.9	$\widehat{H}_N^{(1)}$	0.13640	0.12698	0.11398	0.10982	0.10445	0.1
		$\widehat{H}_N^{(2)}$	0.84039	0.86526	0.87657	0.88378	0.88863	0.9
		$\widehat{\alpha}_N^2$	-Inf	7.38507	6.68990	6.51722	6.39557	6.25
		$\widehat{\beta}_N^2$	Inf	4.15292	3.96086	3.94385	3.93387	4
		$\widehat{\sigma}_N^2$	NaN	0.53650	1.51191	1.78858	1.98559	2.25
		$N_{D\leq 0}$	16	0	0	0	0	-
0.3	0.6	$\widehat{H}_N^{(1)}$	-0.00171	0.16019	0.24138	0.29081	0.31115	0.3
		$\widehat{H}_N^{(2)}$	0.45972	0.62042	0.61246	0.58622	0.58115	0.6
		$\widehat{\alpha}_N^2$	NaN	NaN	NaN	Inf	Inf	6.25
		$\widehat{\beta}_N^2$	NaN	NaN	NaN	-Inf	-Inf	4
		$\widehat{\sigma}_N^2$	NaN	NaN	NaN	NaN	NaN	2.25
		$N_{D\leq 0}$	438	504	437	374	257	-
0.3	0.9	$\widehat{H}_N^{(1)}$	0.33442	0.35563	0.32426	0.31598	0.30505	0.3
		$\widehat{H}_N^{(2)}$	0.82482	0.84811	0.87229	0.88199	0.88805	0.9
		$\widehat{\alpha}_N^2$	-Inf	-Inf	6.79748	7.81230	6.69328	6.25
		$\widehat{\beta}_N^2$	Inf	Inf	4.23064	4.03061	3.95949	4
		$\widehat{\sigma}_N^2$	NaN	NaN	1.13454	0.40685	1.66226	2.25
		$N_{D\leq 0}$	272	66	0	0	0	-
0.4	0.7	$\widehat{H}_N^{(1)}$	0.20770	0.27965	0.30105	0.38415	0.40933	0.4
		$\widehat{H}_N^{(2)}$	0.90791	0.81266	0.71969	0.69097	0.68478	0.7
		$\widehat{\alpha}_N^2$	NaN	NaN	NaN	-Inf	-Inf	6.25
		$\widehat{\beta}_N^2$	NaN	NaN	NaN	Inf	Inf	4
		$\widehat{\sigma}_N^2$	NaN	NaN	NaN	NaN	NaN	2.25
		$N_{D\leq 0}$	275	427	418	340	216	-
0.4	0.9	$\widehat{H}_N^{(1)}$	0.35160	0.46376	0.44752	0.43068	0.40621	0.4
		$\widehat{H}_N^{(2)}$	0.92651	0.85568	0.86091	0.87798	0.88737	0.9
		$\widehat{\alpha}_N^2$	NaN	NaN	-Inf	-Inf	12.64700	6.25
		$\widehat{\beta}_N^2$	NaN	NaN	Inf	Inf	3.99650	4
		$\widehat{\sigma}_N^2$	NaN	NaN	NaN	NaN	-4.32847	2.25
		$N_{D\leq 0}$	346	322	99	10	0	-
0.6	0.9	$\widehat{H}_N^{(1)}$	0.15128	0.21842	0.38914	0.53031	0.59920	0.6
		$\widehat{H}_N^{(2)}$	1.01443	1.02517	0.95966	0.89890	0.89306	0.9
		$\widehat{\alpha}_N^2$	NaN	NaN	3.59861	5.08506	6.32351	6.25
		$\widehat{\beta}_N^2$	NaN	NaN	3.45826	3.75565	3.77811	4
		$\widehat{\sigma}_N^2$	NaN	NaN	5.10517	3.40917	2.21334	2.25
		$N_{D\leq 0}$	10	2	0	0	0	-
0.7	0.9	$\widehat{H}_N^{(1)}$	0.16272	0.24232	0.45009	0.61351	0.69763	0.7
		$\widehat{H}_N^{(2)}$	0.99948	1.04742	1.00428	0.91707	0.90470	0.9
		$\widehat{\alpha}_N^2$	NaN	-Inf	6.49416	0.80762	5.64549	6.25
		$\widehat{\beta}_N^2$	NaN	Inf	4.25616	4.18316	3.61739	4
		$\widehat{\sigma}_N^2$	NaN	NaN	1.40784	7.25799	3.05126	2.25
		$N_{D\leq 0}$	20	1	0	0	0	-

valued averages (Inf, -Inf, or NaN), namely $(0.3, 0.6)$ and $(0.4, 0.7)$; and (3) those producing numerical but physically invalid averaged values, exemplified by the negative $\widehat{\sigma}_N^2$ for $(0.1, 0.6)$ and $(0.4, 0.9)$. We begin with the simplest case, Category (1). In these scenarios, where the count of non-positive discriminants is zero ($N_{D\leq 0} = 0$) at $q = 22$, the estimators demonstrate clear convergence toward the true parameter values. Regarding Category (2), the special-valued averages correspond directly to the occurrence of non-positive discriminants. As evident from the table, the presence of such paths invariably results in Inf, -Inf, or NaN averaged values. This dependency arises because the special-valued averages stem from singularities intrinsic to the estimator formulas: the denominators vanish when $\widehat{x}_N = \widehat{y}_N$, a condition occurring precisely when $\widehat{D}_N \leq 0$. Due to the algebraic structure, $\widehat{u}_N$ and $\widehat{v}_N$ diverge with opposite signs. This causes $\widehat{\alpha}_N^2$ and $\widehat{\beta}_N^2$ to diverge in opposite directions (averaging to NaN if both signs appear), while $\widehat{\sigma}_N^2$, which involves the sum $\widehat{u}_N + \widehat{v}_N$, encounters an indeterminate form directly within individual trajectories. Consequently, any occurrence of a non-positive discriminant invariably results in a NaN average for $\widehat{\sigma}_N^2$. We observe in Table 2 that $N_{D\leq 0}$ decreases significantly as q increases. It is expected that as $N_{D\leq 0}$ reaches zero, the estimators in Category (2) are likely to produce numerical values that are not Inf, -Inf, or NaN, similar to Category (1) or (3). Similarly, as q increases further, the estimators in Category (3) will eventually mirror the convergence behavior of Category (1).

In summary, we have verified the strong consistency of the estimator vector $\widehat{\theta}$. However, the convergence behavior is not uniform across all cases; while many parameter pairs demonstrate rapid convergence within the tested sample sizes, others exhibit slower asymptotic behavior. This variability is primarily driven by the specific values of H_1 and H_2. A detailed analysis of their impact on estimator performance is provided in the next subsection.

4.2 Impact of Hurst Parameters

This subsection examines the impact of H_1 and H_2 on estimation accuracy. Although theoretical convergence is guaranteed as $N \to \infty$, we fix $q = 22$ for this analysis, as it allows for a clear observation of the estimators' behavior across all cases. We present averaged values for a comprehensive set of (H_1, H_2) pairs, covering all possible one-decimal-place combinations. The results are summarized in Table 3.

The first observation is that $N_{D\leq 0}$ is significantly influenced by the values of H_1 and H_2, tending to be higher when both indices are close to 0.5. This trend is notably observed in the $(0.4, 0.6)$ pair, which yields the highest count, followed by the $(0.3, 0.6)$ and $(0.4, 0.7)$ pairs. Next, we examine the impact of index placement by comparing parameter pairs with equivalent relative distances from 0.5 in two distinct scenarios: first, where both indices in one pair are above 0.5 while those in the other are below 0.5; and second, where the indices in both pairs straddle 0.5. In the first scenario, comparing $(0.3, 0.4)$ with $(0.6, 0.7)$ reveals that the former yields a positive $N_{D\leq 0}$ while the latter does not. This discrepancy arises from the property of fBm, which exhibits short-range dependence if $H < 0.5$ and long-range dependence if $H > 0.5$. In the second scenario, comparing $(0.2, 0.6)$ with $(0.4, 0.8)$ shows that despite having symmetric distances from 0.5, the pair containing the smaller

Table 3. Consolidated averaged values of $\widehat{H}_N^{(1)}$, $\widehat{H}_N^{(2)}$, $\widehat{\alpha}_N^2$, $\widehat{\beta}_N^2$, $\widehat{\sigma}_N^2$, and $\widehat{\mu}_N$, along with the count $N_{D\leq 0}$, across 1000 Monte Carlo paths with fixed $q = 22$ for all possible one-decimal-place combinations of (H_1, H_2). The true parameters are $\mu = 0.5, \sigma = 1.5, \alpha = 2.5$, and $\beta = 2$, with $h = 1$.

					$\alpha^2 = 6.25$	$\beta^2 = 4$	$\sigma^2 = 2.25$	$\mu = 0.5$
H_1	H_2	$N_{D\leq 0}$	$\widehat{H}_N^{(1)}$	$\widehat{H}_N^{(2)}$	$\widehat{\alpha}_N^2$	$\widehat{\beta}_N^2$	$\widehat{\sigma}_N^2$	$\widehat{\mu}_N$
0.1	0.2	0	-0.13898	0.44353	3.39753	6.60623	2.49600	0.50001
0.1	0.3	0	-0.03021	0.41950	5.26270	5.10820	2.12890	0.50001
0.1	0.4	0	0.05219	0.44400	5.46431	5.48453	1.55097	0.50001
0.1	0.6	0	0.10310	0.59656	6.48040	24.41960	-18.40020	0.50001
0.1	0.7	0	0.10086	0.69894	6.30313	4.09650	2.09990	0.50005
0.1	0.8	0	0.10192	0.79745	6.31090	4.05312	2.12702	0.50039
0.1	0.9	0	0.10445	0.88863	6.39560	3.93390	1.98560	0.50250
0.2	0.3	0	-0.09316	0.49072	2.88992	7.17183	2.43802	0.50001
0.2	0.4	0	-0.02271	0.61224	4.63092	4.33756	3.53132	0.50001
0.2	0.6	40	0.21117	0.58796	Inf	-Inf	NaN	0.50001
0.2	0.7	0	0.20160	0.69818	6.44523	4.22646	1.82785	0.50005
0.2	0.8	0	0.20241	0.79715	6.37746	4.07148	2.04210	0.50039
0.2	0.9	0	0.20461	0.88839	6.46861	3.94400	1.90242	0.50250
0.3	0.4	3	-0.00897	0.57838	NaN	NaN	NaN	0.50000
0.3	0.6	257	0.31115	0.58115	Inf	-Inf	NaN	0.50001
0.3	0.7	4	0.30522	0.69448	-Inf	Inf	NaN	0.50005
0.3	0.8	0	0.30368	0.79648	6.75973	4.12136	1.60995	0.50039
0.3	0.9	0	0.30505	0.88805	6.69330	3.95950	1.66230	0.50250
0.4	0.6	422	0.35978	0.60931	NaN	NaN	NaN	0.49999
0.4	0.7	216	0.40933	0.68478	-Inf	Inf	NaN	0.50004
0.4	0.8	6	0.40921	0.79286	-Inf	Inf	NaN	0.50038
0.4	0.9	0	0.40621	0.88737	12.64700	3.99650	-4.32850	0.50249
0.6	0.7	0	0.19286	0.94475	3.61876	5.36072	3.52011	0.49981
0.6	0.8	0	0.52956	0.83954	2.92350	3.60819	5.95937	0.50014
0.6	0.9	0	0.59920	0.89306	6.32350	3.77810	2.21330	0.50226
0.7	0.8	0	0.45191	0.98358	4.69889	4.66727	3.12427	0.49938
0.7	0.9	0	0.69763	0.90470	5.64550	3.61740	3.05130	0.50149
0.8	0.9	0	0.65877	1.10091	6.08115	3.76690	2.45202	0.49844

index 0.2 yields a significantly higher count. Consequently, $N_{D\leq 0}$ tends to be higher for the pair containing an index that deviates further below 0.5.

The second important observation is that the averaged values of $\widehat{H}_N^{(1)}$ and $\widehat{H}_N^{(2)}$ exhibit larger deviations from the true values when H_1 and H_2 are close to each other. This behavior is clearly visible across the pairs $(0.6, 0.7)$, $(0.6, 0.8)$, and $(0.6, 0.9)$. We observe that the averaged values deviate most for the closest pair, $(0.6, 0.7)$, but become progressively closer to the true parameters as the indices become more distant, resulting in accurate averaged values for the most separated pair, $(0.6, 0.9)$. Furthermore, even when the distance between the indices is identical, parameter pairs where both values are below 0.5 exhibit larger deviations from the true parameters compared to pairs where both indices exceed 0.5. This is evident when comparing $(0.1, 0.3)$ with $(0.7, 0.9)$; the former yields poor averaged values (-0.030 and 0.420), while the latter is precise (0.698 and 0.905). A similar pattern is observed for other pairs with equivalent separations, such as $(0.1, 0.4)$ versus $(0.6, 0.9)$ and $(0.2, 0.4)$ versus $(0.6, 0.8)$. This phenomenon arises from the dependence properties of fBm. In summary, the accuracy of the estimators tends to deteriorate significantly when the two Hurst parameters are close to each other or when both are below 0.5. Revisiting the results in Table 2, the negative averaged estimates observed for the (0.1,0.3) pair can be attributed to this Hurst parameter effect. However, by the strong consistency result, the estimates are guaranteed to converge to the true parameter as the sample size increases. This asymptotic behavior becomes evident at $q = 22$, where the averaged estimate moves noticeably closer to the true parameter.

The third key observation concerns the coefficient estimators $\widehat{\alpha}_N^2$, $\widehat{\beta}_N^2$, and $\widehat{\sigma}_N^2$, corresponding to B^{H_1}, B^{H_2}, and W, respectively. Having addressed the special-valued cases, we now focus on the valid numerical values. We find that estimation accuracy is fundamentally governed by the relative distinctness among H_1, H_2, and the Brownian index 0.5. When any pair of these values is close, their corresponding stochastic components exhibit similar dynamics, confounding the identification of their coefficients. To illustrate this, we examine three representative cases characterized by different proximity patterns: Case (1), where $H_1 = 0.4$ is close to the Brownian index 0.5 while $H_2 = 0.9$ is distant; Case (2), where $H_2 = 0.6$ is close to 0.5 while $H_1 = 0.1$ is distant; and Case (3), where $H_1 = 0.1$ and $H_2 = 0.2$ are close to each other but well-separated from 0.5. In the first two cases, the proximity of a Hurst index to the Brownian index results in substantial errors for the pair $\widehat{\sigma}_N^2$ and $\widehat{\alpha}_N^2$ in Case (1), and the pair $\widehat{\sigma}_N^2$ and $\widehat{\beta}_N^2$ in Case (2), while the estimator for the distant component remains robust. In Case (3), the distinctness of the Brownian index 0.5 from both fractional indices allows $\widehat{\sigma}_N^2$ to remain reliable, whereas $\widehat{\alpha}_N^2$ and $\widehat{\beta}_N^2$ may still suffer from mutual confounding. Furthermore, despite identical separations, pairs below 0.5 exhibit larger deviations than those above 0.5, as exemplified by the comparisons of $(0.1, 0.4)$ versus $(0.6, 0.9)$ and $(0.1, 0.2)$ versus $(0.8, 0.9)$.

The final key observation is that the trend estimator $\widehat{\mu}_N$ is robust across all (H_1, H_2) pairs. However, a comparison of cases with a fixed H_1 reveals that av-

eraged values corresponding to $H_2 = 0.9$ consistently exhibit the largest deviation from the true value. This occurs because as the Hurst index increases, the fBm produces paths that become progressively smoother, thereby closely mimicking a linear trend.

In summary, the accuracy of the estimators depends heavily on the values of H_1 and H_2. The estimators tend to exhibit increased errors when the indices are close to each other or near 0.5. Although the estimators are theoretically consistent, these challenging cases require significantly larger sample sizes to achieve accurate results.

4.3 Effect of Function Selection for $\widehat{\sigma}^2$

As discussed in Section 3, estimators for σ^2 can be constructed using various Borel functions. In this subsection, we examine the family of estimators $\widehat{\sigma}^2_{k,N}$ for $k = 1, \ldots, 6$. We will numerically demonstrate the strong agreement among these estimators using two complementary approaches. First, we analyze how the discrepancies between the estimators evolve as the sample size exponent q increases. Second, we present estimated values for individual simulation paths to directly illustrate the closeness of the estimates. Throughout this analysis, we fix the model parameters at $\mu = 0.5, \sigma = 1.5, \alpha = 2.5, \beta = 2.0, H_1 = 0.1$, and $H_2 = 0.9$.

To implement the first approach, we conducted a Monte Carlo simulation study varying the parameter q across the values $14, 16, 18, 20, 22$. For each of the 1000 generated paths, we computed the *range* of the estimates by calculating the difference between the maximum and minimum values obtained from all six estimators. The averages of these ranges are summarized in Table 4. The results demonstrate a clear decreasing trend, confirming that although discrepancies may be pronounced at smaller sample sizes, they diminish as the sample size increases, and the estimators asymptotically converge to a unified value.

We address the second objective by examining the estimated values for individual simulation paths. Throughout our simulations, we consistently observe that while estimates may deviate from the true parameter value, these six different estimators exhibit a uniform pattern of deviation. To illustrate this general behavior, Table 5 presents the results for five representative independent trajectories. Notably, estimators derived from the quadratic functions ($\widehat{\sigma}^2_{1,N}$ to $\widehat{\sigma}^2_{5,N}$) yield results that are nearly identical, whereas the estimator derived from the cubic function ($\widehat{\sigma}^2_{6,N}$) differs slightly yet remains within an acceptable range.

In conclusion, the results demonstrate a clear dependency on the sample size exponent q. The discrepancies among the six estimators are amplified at lower sample sizes. However, the average range decreases monotonically as q increases, validating the asymptotic convergence of all estimators. This means that while the choice of function can slightly impact the estimate at limited sample sizes, the overall findings indicate that the influence of the function selection becomes negligible as $N \to \infty$. Furthermore, as noted in Remark 3.3, although an alternative equation could be employed to estimate σ^2 within the estimator vectors in Theorems 3.1 and 3.2, the results would remain consistent with the asymptotic behavior observed here.

4.4 Comparison of Proposed Estimators

Following the analysis where only the estimator for σ^2 was modified, we now extend our comparison to the full estimator

Table 4. Averaged range of estimates for $\widehat{\sigma}^2_{k,N}$ $(k = 1, \ldots, 6)$ across 1000 Monte Carlo paths with varying q. The true parameters are $\mu = 0.5, \sigma = 1.5, \alpha = 2.5, \beta = 2, H_1 = 0.1$, and $H_2 = 0.9$, with $h = 1$.

q	14	16	18	20	22
Average Range	NaN	0.9773	0.5190	0.2002	0.1819

Table 5. Estimates obtained using $\widehat{\sigma}^2_{k,N}$ $(k = 1, \ldots, 6)$ across five representative independent simulation paths with fixed $q = 22$. The true parameters are $\mu = 0.5, \sigma = 1.5, \alpha = 2.5, \beta = 2, H_1 = 0.1$, and $H_2 = 0.9$, with $h = 1$.

$\widehat{\sigma}^2_{1,N}$	$\widehat{\sigma}^2_{2,N}$	$\widehat{\sigma}^2_{3,N}$	$\widehat{\sigma}^2_{4,N}$	$\widehat{\sigma}^2_{5,N}$	$\widehat{\sigma}^2_{6,N}$
2.2253287	2.2253304	2.2253291	2.2252986	2.2251340	2.2734313
1.8626352	1.8625612	1.8625786	1.8628086	1.8633384	1.8628291
2.2417247	2.2417274	2.2417156	2.2416714	2.2415880	2.3908448
2.6743607	2.6743356	2.6743426	2.6743540	2.6744836	2.7016142
0.2601327	0.2601406	0.2601360	0.2601335	0.2599453	0.2814503

vectors: $\widehat{\theta}$ (from Theorem 2.3), $\widetilde{\theta}$ (from Theorem 3.1), and $\breve{\theta}$ (from Theorem 3.2). Since the estimator for μ remains identical across all vectors, our focus narrows to the five remaining parameters. We assess the agreement among these three vectors using two complementary approaches: first, by analyzing the evolution of discrepancies among the estimators as the sample size exponent q increases; and second, by examining estimated values from individual simulation paths to directly visualize their proximity.

To implement the first approach, we conducted a Monte Carlo simulation study varying the parameter q across the values $14, 16, 18, 20, 22$, while fixing the model parameters at $\mu = 0.5, \sigma = 1.5, \alpha = 2.5, \beta = 2.0, H_1 = 0.1$, and $H_2 = 0.9$. For each of the 1000 generated paths, we computed the range of the estimates for the five distinct parameters. The averages of these ranges are summarized in Table 6. The results exhibit a clear decreasing trend, confirming that while discrepancies are more pronounced at smaller sample sizes, they diminish consistently as the sample size increases. This provides strong evidence that the estimators from all three theorems asymptotically converge to a unified value.

We address the second objective by examining estimates obtained from various parameter sets at a fixed sample size exponent of $q = 22$. Consistent patterns of agreement are observed across all investigated scenarios. Three representative parameter sets were selected as illustrative examples, whose results from a single simulation path are presented in Table 7. The table displays the true parameter values in the first column, followed by the estimates obtained using $\widehat{\theta}$, $\widetilde{\theta}$, and $\breve{\theta}$. The results mirror the patterns observed in the previous analysis: even when an individual trajectory yields deviations from the true parameters, their estimates remain remarkably close to one another. This confirms that for sufficiently large q, the choice of the equation system has minimal impact on the estimation results.

In conclusion, the comparative analysis of $\widehat{\theta}$, $\widetilde{\theta}$, and $\breve{\theta}$ confirms their significant numerical agreement and consistent asymptotic behavior. As evidenced by the simulation results, while discrepancies and occasional numerical instabilities

Table 6. Averaged range of estimates for H_1, H_2, α^2, β^2, and σ^2 across the estimator vectors $\widehat{\theta}, \widetilde{\theta}$, and $\breve{\theta}$ over 1000 Monte Carlo paths with varying q. The true parameters are $\mu = 0.5, \sigma = 1.5, \alpha = 2.5, \beta = 2, H_1 = 0.1$, and $H_2 = 0.9$, with $h = 1$.

Parameter	q				
	14	16	18	20	22
H_1	3.994×10^{-3}	8.857×10^{-4}	2.145×10^{-4}	5.027×10^{-5}	1.280×10^{-5}
H_2	1.804×10^{-3}	3.403×10^{-4}	7.594×10^{-5}	1.687×10^{-5}	4.144×10^{-6}
α^2	NaN	2.831×10^{-2}	5.052×10^{-3}	1.102×10^{-3}	2.706×10^{-4}
β^2	NaN	1.188×10^{-2}	2.329×10^{-3}	5.033×10^{-4}	1.224×10^{-4}
σ^2	NaN	4.024×10^{-2}	7.392×10^{-3}	1.608×10^{-3}	3.939×10^{-4}

Table 7. Comparison of parameter estimates obtained using $\widehat{\theta}$, $\widetilde{\theta}$, and $\breve{\theta}$ from a single simulation path for each of three representative parameter sets, with fixed $q = 22$.

Parameter	$\widehat{\theta}$	$\widetilde{\theta}$	$\breve{\theta}$
$H_1 = 0.1$	0.1048506	0.1047530	0.1047762
$H_2 = 0.9$	0.8908218	0.8908533	0.8908458
$\alpha^2 = 6.25$	6.4469250	6.4448455	6.4453404
$\beta^2 = 4$	3.9366163	3.9356864	3.9359077
$\sigma^2 = 2.25$	1.9602925	1.9632960	1.9626457
$H_1 = 0.1$	0.1095725	0.1091502	0.1092836
$H_2 = 0.3$	0.3480623	0.3476878	0.3478058
$\alpha^2 = 0.0225$	0.0326550	0.0325311	0.0325702
$\beta^2 = 0.0625$	0.0580209	0.0581066	0.0580796
$\sigma^2 = 0.04$	0.0345079	0.0345461	0.0345342
$H_1 = 0.7$	0.6394608	0.6398109	0.6396807
$H_2 = 0.9$	0.8708606	0.8709079	0.8708903
$\alpha^2 = 1$	0.7345192	0.7343801	0.7344310
$\beta^2 = 1$	1.2551387	1.2543348	1.2546340
$\sigma^2 = 1$	0.9569409	0.9578841	0.9575413

(indicated by NaN values) are observable at smaller sample sizes, they diminish rapidly as q increases, demonstrating strong convergence across all estimator vectors. Furthermore, regarding computational efficiency, the execution times for all three estimator vectors were found to be comparable. A similar observation holds for the estimators $\widehat{\sigma}^2_{k,N}$ $(k = 1, \ldots, 6)$, which also exhibited negligible differences in computational cost. However, when applying these estimator vectors to real-world data characterized by limited sample sizes, determining the optimal choice remains challenging, as relative performance depends heavily on the specific characteristics of the underlying series. This variability and data dependency are further illustrated in the subsequent section.

5. Application to Cryptocurrency Data

Asset price forecasting has traditionally relied on geometric Brownian motion (gBm) due to its analytical tractability. However, financial time series often exhibit persistent correlations, which the independent increments of Bm fail to capture. To address this limitation, fBm has been incorporated, leading to the geometric mixed fractional Brownian motion (gmfBm). In this study, we extend this framework by introducing the geometric Brownian motion mixed with two fractional Brownian motions (gBm2fBm). This model provides enhanced flexibility in capturing the heterogeneous dependence structures observed in real markets. We define the models directly via their logarithmic price representations:

gBm:

$$\log\left(\frac{S_t}{S_0}\right) = \left(\mu - \frac{1}{2}\sigma^2\right)t + \sigma W_t,$$

gmfBm:

$$\log\left(\frac{S_t}{S_0}\right) = \mu t + \sigma W_t + \alpha B_t^{H_1},$$

gBm2fBm:

$$\log\left(\frac{S_t}{S_0}\right) = \mu t + \sigma W_t + \alpha B_t^{H_1} + \beta B_t^{H_2},$$

where S_t denotes the asset price at time t, and $W_t, B_t^{H_1}$, and $B_t^{H_2}$ are mutually independent. For the gmfBm and gBm2fBm models defined above, we make no assumption regarding the stochastic integral interpretation. However, under the Itô interpretation, μ is effectively replaced by $(\mu - \frac{1}{2}\sigma^2)$, from which μ is easily recovered via algebraic rearrangement.

We focus on the daily closing prices of the SOL token, sourced from Yahoo Finance, a cryptocurrency selected for its high liquidity and distinct volatility patterns. The estimation period spans from October 24, 2023, to July 20, 2025, comprising a total of 636 observations. Using the estimated parameters, we simulate 1000 trajectories for each model that yields valid parameters, employing conditional expectation to preserve the dependency structure inherent in the fractional components. The predictive accuracy of these simulations is then evaluated against the actual data from July 21, 2025, to September 18, 2025. The estimator vector for the gBm model, denoted as $\acute{\theta} = (\acute{\mu}, \acute{\sigma})$, is obtained following Ibrahim et al. [6], while that for the gmfBm model, denoted as $\grave{\theta} = (\grave{\mu}, \grave{\sigma}, \grave{\alpha}, \grave{H})$, is estimated following Kukush et al. [16]. For the gBm2fBm model, we apply the three estimator vectors $\widehat{\theta}, \widetilde{\theta}, \breve{\theta}$ derived in this work. The estimated parameters are reported in Table 8. We observe that the gmfBm model yields a negative Hurst index ($H = -0.084$), violating the theoretical condition $H \in (0, 1)$. Similarly, the alternative gBm2fBm estimators $\widetilde{\theta}$ and $\breve{\theta}$ produce invalid results for this specific dataset, yielding imaginary volatility coefficients and non-positive Hurst indices. These anomalies serve as empirical evidence of the estimation challenges discussed in Section 4, which may arise from the occurrence of a non-positive discriminant in the observed trajectory or deviations from the model's underlying assumptions. Consequently, for the simulation and error analysis, we proceed using only the valid estimates from $\widehat{\theta}$ for the gBm2fBm model, alongside the standard gBm model.

The simulation results derived from these two models are presented in Figs. 2-3. Fig. 2 presents a comparison between ten randomly selected simulated paths and the actual historical data. To provide a comprehensive view, all simulated trajectories are plotted in Fig. 3. As evident from these plots, the trajectories generated by the gBm and gBm2fBm models are visually indistinguishable. Given this visual resemblance, we evaluate predictive performance using the Mean Absolute Percentage Error (MAPE) and Root Mean Squared Percentage Error (RMSPE), calculated via two averaging approaches: *Mean-then-Error* (error of the averaged path) and *Error-then-Mean* (average of individual path errors). As detailed in Table 9, the gBm2fBm model $(\widehat{\theta})$ consistently yields lower errors than the gBm model across all metrics, indicating superior predictive accuracy for this dataset.

In summary, this study evaluates the practical performance of the proposed estimators using daily closing prices of the SOL token, benchmarking the gBm2fBm model against gBm and gmfBm. While the gmfBm model and the alternative gBm2fBm estimator vectors $(\widetilde{\theta}, \breve{\theta})$ yielded theoretically invalid parameters for the analyzed series, the gBm2fBm estimator vector $\widehat{\theta}$ remained valid and demonstrated superior predictive accuracy. However, estimator validity and performance are highly sensitive to data characteristics. Extended testing on other assets, such

Table 8. Estimated parameters for each model based on SOL token data.

Model	Estimator	Parameter					
		μ	σ	α	β	H_1	H_2
gBm	$\acute{\theta}$	0.003	0.047	—	—	—	—
gmfBm	$\grave{\theta}$	0.003	0.045	0.012	—	-0.084	—
gBm2fBm	$\widehat{\theta}$	0.003	0.038	0.017	0.023	0.137	0.543
	$\widetilde{\theta}$	0.003	0.046	$0.0004i$	0.012	0.000	-0.138
	$\breve{\theta}$	0.003	0.046	$0.0004i$	0.012	0.000	-0.145

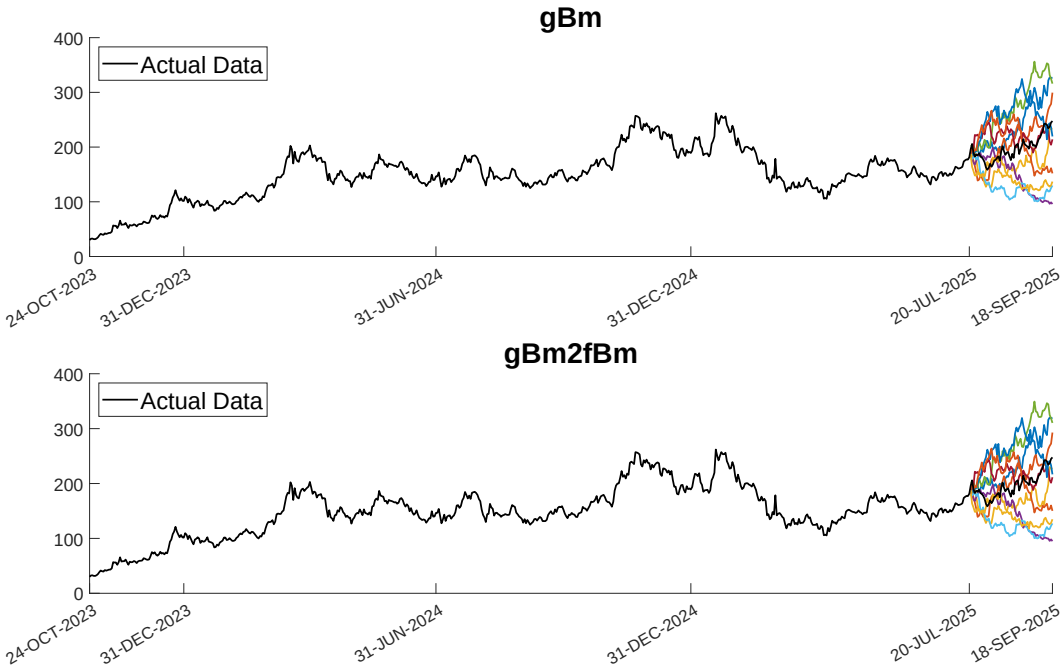


Fig. 2. Comparison of ten simulated paths with the actual observed data.

Table 9. Percentage errors for the gBm and gBm2fBm models under two averaging approaches.

Criterion	gBm	gBm2fBm ($\widehat{\theta}$)
MAPE (Mean-then-Error)	7.1923	6.7612
MAPE (Error-then-Mean)	21.802	21.302
RMSPE (Mean-then-Error)	0.8828	0.8350
RMSPE (Error-then-Mean)	2.5511	2.4933

as BTC and RENDER, confirmed this variability, as either the proposed gBm2fBm model or the simpler gBm model proved superior depending on the specific dataset and time interval. Therefore, rather than claiming universal dominance, we present the gBm2fBm model as a valuable alternative for modeling asset prices.

6. Discussion and Conclusion

This study applies the ergodic theorem to estimate the parameters of the BmT2fBm model. Our theoretical and numerical investigations yield three key insights.

First, we conclude that the choice of Borel functions for constructing the estimators does not significantly impact the

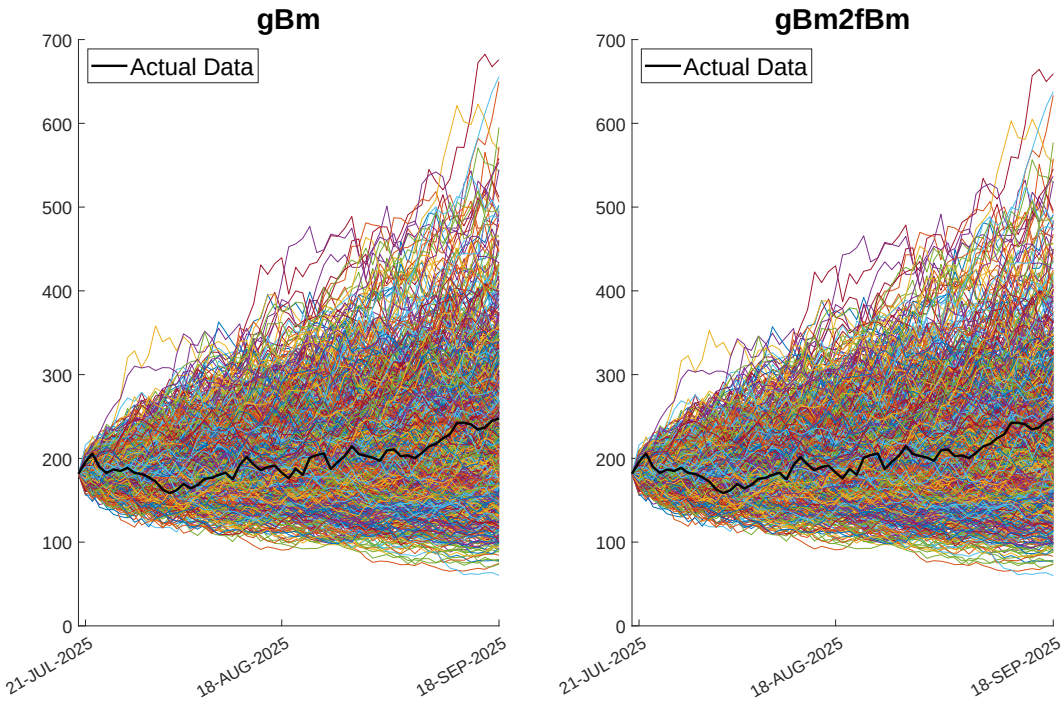


Fig. 3. Comparison of the full set of simulated trajectories (1000 paths) with the actual data.

results when the sample size is sufficiently large. The estimator vectors derived from different Borel function selections yield estimates that remain remarkably close to one another, confirming the robustness of the estimation method based on the ergodic theorem. However, establishing the precise theoretical rate of convergence for these estimators remains an open question that would provide valuable insights for future research.

Second, while strong consistency is guaranteed as $N \to \infty$, finite-sample performance is critically sensitive to the configuration of the Hurst indices. Our simulations reveal that estimation errors and numerical instabilities, manifesting as non-positive discriminants or undefined (NaN) coefficients, are most prevalent when H_1 and H_2 are in close proximity to each other or to the Brownian limit of 0.5. In such regimes, significantly larger sample sizes are required to achieve robust convergence compared to other configurations.

Finally, the empirical application to cryptocurrency data highlights the predictive superiority of the gBm2fBm model over standard benchmarks like gBm. However, real-world data can trigger theoretical singularities, resulting in invalid parameters for certain estimator vectors. Therefore, the gBm2fBm model offers a viable alternative for modeling asset prices or processes potentially characterized by the interplay of Brownian and fractional stochastic drivers. However, its suitability is not guaranteed in advance and thus requires empirical verification. Practitioners are advised to first estimate the model parameters for the dataset; the occurrence of invalid estimates (e.g., $H \notin (0,1)$ or non-real coefficients) may indicate that the sample size is insufficient, the model is misspecified, or the chosen estimation

framework is unsuitable for the underlying process.

Despite these contributions, the present framework has certain theoretical limitations that suggest directions for future research. Currently, the model relies on the assumption that the driving stochastic processes (W, B^{H_1}, and B^{H_2}) are mutually independent and that the observations are collected at regularly spaced time intervals. In many practical applications, such as financial markets, these assumptions may be restrictive due to potential dependence structures and irregular sampling schemes. Therefore, future work could extend the proposed estimation framework to settings with correlated driving processes. In addition, adapting the methodology to irregularly spaced observations or extending the model to a multivariate setting would be natural and promising directions for further research.

References

[1] Kolmogorov AN. Wienersche Spiralen und einige andere interessante Kurven im Hilbertschen Raum. C R (Doklady) Acad Sci URSS (NS) 1940;26:115-8.

[2] Biagini F, Hu Y, Øksendal B, Zhang T. Stochastic calculus for fractional Brownian motion and applications. London: Springer; 2008.

[3] Mishura YS. Stochastic calculus for fractional Brownian motion and related processes. Berlin: Springer; 2008.

[4] Rostek S, Schöbel R. A note on the use of fractional Brownian motion for financial modeling. Econ Model 2013;30:30-5.

[5] Decreusefond L, Üstünel AS. Fractional Brownian motion: theory and applications. ESAIM Proc 1998;5:75-86.

[6] Ibrahim SNI, Misiran M, Laham MF. Geometric fractional Brownian motion model for commodity market simulation. Alex Eng J 2021;60:955-62.

[7] Kubilius K, Skorniakov V, Melichov D. Estimation of parameters of SDE driven by fractional Brownian motion with polynomial drift. J Stat Comput Simul 2016;86:1954-69.

[8] Cheridito P. Mixed fractional Brownian motion. Bernoulli 2001;7:913-34.

[9] Filatova D. Mixed fractional Brownian motion: some related questions for computer network traffic modeling. In: Int Conf Signals Electron Syst; 2008. p. 393-6.

[10] Sun L. Pricing currency options in the mixed fractional Brownian motion. Phys A: Stat Mech Appl 2013;392:3441-58.

[11] Zhang WG, Xiao WL, He CX. Equity warrants pricing model under fractional Brownian motion and an empirical study. Expert Syst Appl 2009;36:3056-65.

[12] Xiao WL, Zhang WG, Zhang X. Maximum-likelihood estimators in the mixed fractional Brownian motion. Statistics 2011;45:73-85.

[13] Zhang P, Sun Q, Xiao WL. Parameter identification in mixed Brownian-fractional Brownian motions using Powell's optimization algorithm. Econ Model 2014;40:314-9.

[14] Dozzi M, Mishura Y, Shevchenko G. Asymptotic behavior of mixed power variations and statistical estimation in mixed models. Stat Inference Stoch Process 2015;18:151-75.

[15] Dufitinema J, Pynnönen S, Sottinen T. Maximum likelihood estimators from discrete data modeled by mixed fractional Brownian motion with application to the Nordic stock markets. Commun Statist Simulation Comput 2022;51:5264-87.

[16] Kukush A, Lohvinenko S, Mishura Y, Ralchenko K. Two approaches to consistent estimation of parameters of mixed fractional Brownian motion with trend. Stat Inference Stoch Process 2022;25:159-87.

[17] Miao Y, Ren W, Ren Z. On the fractional mixed fractional Brownian motion. Appl Math Sci (Ruse) 2008;2:1729-38.

[18] Mishura Y. Maximum likelihood drift estimation for the mixing of two fractional Brownian motions. In: Stochastic and Infinite Dimensional Analysis (Trends in Mathematics). Cham: Birkhäuser/Springer; 2016. p. 263-80.

[19] Mishura Y, Voronov I. Construction of maximum likelihood estimator in the mixed fractional-fractional Brownian motion model with double long-range dependence. Mod Stoch Theory Appl 2015;2:147-64.

[20] Ralchenko K, Yakovliev M. Parameter estimation for fractional mixed fractional Brownian motion based on discrete observations. Mod Stoch Theory Appl 2024;11:1-29.

[21] Higham DJ. An algorithmic introduction to numerical simulation of stochastic differential equations. SIAM Rev 2001;43:525-46.

[22] Shevchenko G. Fractional Brownian motion in a nutshell. Int J Mod Phys Conf Ser 2015;36:1560002.

[23] Wood ATA, Chan G. Simulation of stationary Gaussian processes in $[0,1]^d$. J Comput Graph Statist 1994;3:409-32.

[24] Maruyama G. The harmonic analysis of stationary stochastic processes. Memoirs of the Faculty of Science, Kyushu University 1949;4:45-106.

[25] Bennedsen M, Christensen K, Christensen P. To be or not to be: Roughness or long memory in volatility? J Econometrics 2026;254:106193.